FAKULTÄT FÜR !NFORMATIK
Faculty of Informatics

Towards Distributed Controllers Based on Caenorhabditis elegans Locomotory Neural Network

DIPLOMA THESIS

submitted in partial fulfillment of the requirements for the degree of

Diplom-Ingenieur

in

Software Engineering & Internet Computing

by

Ondrej Balún
Registration Number 1328503

to the

Faculty of Informatics at the TU Wien

Supervisor: Univ.Prof. Dipl.-Ing. Dr.rer.nat. Radu Grosu

Co-Supervisor: Dott. Mag. Ramin M. Hasani

Vienna, 31st July, 2016

Ondrej Balún	Radu Grosu

Erklärung zur Verfassung der Arbeit

Ondrej Balún
Lovčica 153, 96623 Lovčica - Trubín, Slovakia

Hiermit erkläre ich, dass ich diese Arbeit selbständig verfasst habe, dass ich die verwendeten Quellen und Hilfsmittel vollständig angegeben habe und dass ich die Stellen der Arbeit – einschließlich Tabellen, Karten und Abbildungen –, die anderen Werken oder dem Internet im Wortlaut oder dem Sinn nach entnommen sind, auf jeden Fall unter Angabe der Quelle als Entlehnung kenntlich gemacht habe.

Wien, 31. Juli 2016

Ondrej Balún

Acknowledgements

I would like to express my gratitude to Professor Radu Grosu and Dott. Mag. Ramin M. Hasani and my colleagues from Cyber-Physical Systems lab at TU Vienna who all provided me with invaluable insight and expertise that greatly assisted this project.

Abstract

In the present study, we aim to understand neuronal controlling mechanisms by investigating the locomotory neural circuit of the nematode Caenorhabditis elegans (C. elegans). C. elegans is a transparent 1mm roundworm which naturally inhabits in soil. Its stereotypic nervous system consists of only 302 identifiable neurons hard-wired through approximately 5000 chemical synapses and 2000 gap junctions. Because of highly concentrated biological research on its neuronal network, C. elegans is one of the promising models to learn the controlling and learning principles applicable in development of brain-inspired artificial intelligence. We are particularly interested in the part of the locomotory neuronal controller – *Tap Withdrawal* (TW) neuronal circuit – responsible for the processing of the mechanical tap stimulus.

We applied synaptic and neuronal "computer" ablations to measure the impact of reducing neuronal structure on time spent on specific direction of locomotion and membrane potential of neurons. The minimal forward- and backward-responsible circuit have been constructed by adding connections from scratch. The minimal circuits are merged to check the modularity of two behavioral opposite circuits.

We have identified crucial chemical and electrical synapses controlling the forward and backward tap withdrawal. We have reduced them to find the minimal number of connections preserving the correct behavioral output. Neuronal ablations emphasize the premier role of the excitatory neurons within the neural circuit. The technique of building the minimal circuits from scratch allowed us to identify functional pathways and cycles responsible for (i) recognizing the start and end of the stimulus, (ii) behavioral concurrency and (iii) structural support for default forward locomotion. By putting two minimal circuits together, we identified overlapping parts of the circuits, crucial for both, anterior and posterior taps.

Finally, based on the acquired knowledge, we introduce a new fashion in designing of neuronal controllers by implementing simple stock market decision module. The decision module is composed of two sub-modules: 1. Indicator evaluation module compares the current and historical value of chosen stock market indicator, 2. C. elegans TW circuit mapping the forward and backward commands to BUY or SELL stocks.

Abstract

In dieser Studie versuchen wir die Neuron-Steuermechanismen zu begreifen in dem, dass wir den Bewegungsnervenkreis der Nematode Caenorhabditis elegans (C. elegans) untersuchen. C. elegans ist ein transparenter 1 mm langer Spulwurm, die üblich im Erdreich vorkommt. Sein stereotypischer Neurosystem besteht aus nur 302 identifizierten Neuronen, die miteinander durch circa 5000 chemischen Synapsen und 2000 elektrischen Synapsen verbunden sind. Hinsichtlich der hochkonzentrierter biologischen Untersuchung seines Neuron-Netzes ist C.elegans einer der vielversprechenden Modelle für die Auffassung der Steuerungsprinzipien und Neuron-Netz-Lehre, die bei der Entwicklung der gehirn-inspizierten künstlichen Intelligenz anwendbar sind. Uns interessiert vor allem der Teil des Bewegungsneurokontrollers - Tap Withdrawal (TW) Neuron-Kreis – der für die Anreizverarbeitung der mechanischen Berührung verantwortlich ist.

Mit Hilfe der synaptischen und Neuron-Ablösungen haben wir die Auswirkung der Strukturreduzierung des Neuron-Netzes auf die Bewegungszeit der C.elegans vorwärts und rückwärts gemessen. Die Minimal-Neuron-Kreise für die Bewegungssteuerung vorwärts und rückwärts wurden mit Hilfe der allmählichen Zugabe der Synapsen von Null auf konstruiert. Folglich wurden diese Minimalkreise miteinander, wegen der Modularitätsanalyse der beiden gegensätzlich sich benehmenden Kreise, integriert. Wir haben die chemischen und elektrischen Synapsen, die für die „tap withdrawal“-Reflex-Steuerung vorwärts und rückwärts schlaggebend sind, identifiziert. Wir experimentierten mit einer Minimalzahl von Synapsen, bei der der geforderte Verhaltensausgang erhalten wurde.

Die Neuron-Ablösungen haben die wichtige Aufgabe der Anregungsneuronen in Neurokreis hervorgehoben. Die Aufbautechnik der Minimalkreise von Null hat uns ermöglicht die Funktionswege und Zyklen, die für (i) Erkennung des Anfangs und Ende des Berührungsanreizes, (ii) konkurrierende Verhaltungsprozesse und (iii) strukturelle Unterstützung der Ausgangsbewegung vorwärts zu identifizieren. Mittels der Verbindung von Minimalkreisen haben wir die überlappenden Kreisteile, die grundlegend für beide Bewegungsrichtungen sind, identifiziert.

Zum Schluss bemühen wir uns, auf Grund der erworbenen Kenntnisse, einen neuen Weg bei der Projektierung der Neuron-Kontroller, mittels der Vorführung eines einfachen Entscheidungsbausteins für den Investor auf der Aktienbörse, vorzustellen. Der Entscheidungsbaustein besteht aus zwei Teilbausteinen: 1. Vergleichsbaustein für den Vergleich eines aktuellen und historischen Wertes des gewählten Indikators der Aktienbörse, 2. C.

elegans TW-Modul für Bewegungsabbildung der Vorwärts- und Rückwärtsbewegung auf die Anweisungen des Aktienkaufes oder Aktienverkaufes.

Contents

CHAPTER 1

Introduction

In this research work, we aim to extract elegant neuronal control principles by investigating the locomotory neural circuit of the nematode Caenorhabditis elegans (C. elegans). Recently, there is huge demand for brain-inspired artificial intelligence (AI) solutions in the field of applied computer science [1]. First step towards developing brain-like high-tech is deep understanding of the working principles of the biological neural networks (BNN)s. Studying the simple BNNs is the necessary precondition on understanding of more complex networks.

One of the highly concentrated researches on BNNs, is the brain of the C. elegans [2, 3, 4, 5, 6, 7, 8]. C. elegans is a 1mm soil roundworm easy maintainable in the laboratory environment. Its simple nervous system consists of 302 neurons hard-wired through approximately 5000 chemical synapses and 3000 gap junctions which has been mapped initially in [4]. The network comprises several neural circuits (NC)s each of which responsible for a behavioral task in the worm. For instance, the worm is able to move as a result of the existence of the locomotory NC. The working principle of the locomotory NC has been researched in various biological researches and therefore is a suitable neural network to be investigated [3, 4, 7, 9, 10, 11]. One of the key strength of such network is the ability of massive parallel data processing from multiple sensory data to motor stimulation.

We are particularly interested in the part of the locomotory NC – *Tap Withdrawal* (TW) neuronal circuit – responsible for the processing of the mechanical tap stimulus [12]. The C. elegans responses to the tap stimulus with the *withdrawal*, which can be interpreted as an escape from potentially dangerous environment.

The first investigation on TW circuit with the goal of identifying of the neurons responsible for the initiating of the reverse movement as a response to the anterior tap and the neurons responding to the posterior tap with forward acceleration has been done with the help of laser ablations by Chalfie et al. in 1985 [3]. The neuronal wiring diagram

described in [4] has been further reused by Wicks et al. in 1995 [9] in order to identify the mechanosensory cells and interneurons building two concurrent sub-circuits governing the forward and backward locomotion. The dynamics of the membrane potential of neurons has been described applying the mathematical model in [2] in order to estimate the polarities of the neurons. The model comprises a system of nonlinear ODEs simulating the internal state of the neuron and the currents flowing into the neuron through the chemical synapses, gap junctions and external stimulation.

Although the physiological structure of the TW circuit is known for decades, deep understanding of the working principles behind the neurons and synapses is yet missing. Studying the simple neuronal pathways and subcircuits of the TW circuit can lead to implementation of novel parallel data processing, new sets of decision making algorithms and distributed control models while employing robust design. Furthermore, the extracted knowledge can be reused in design of the biologically inspired neural controllers which are applicable in various AI control systems. Such controllers potentially outperform the artificial-neural-network-based controllers where it replace the hidden black-box layer of the ANNs with fully traceable structure.

Here, in order to understand the features of the TW circuit, the most important chemical synapses and gap junctions are identified by studying the impact of the step-wise "computer" ablations (knocking out the synapses one by one). As a results, an abstract TW NC is realized by employing the essential connections. We describe in details the high degree of robustness of this NC in the process of synapse and neuron ablation. Minimal circuits for the forward and backward locomotion are constructed with the aim of clarifying the key concepts of sensing, processing and evaluating the tap stimulus. Moreover, such abstracts are merged into one minimal TW circuit in order to study the modularity of the subcircuits and their interference when they are combined together. We justify our results on the roles of the neurons, synapses and gap junctions by comparing them to the outcome of similar biological experiments.

In case of anterior tap, the backward-responsible circuits cross-inhibits the forward-responsible circuit in order to gain control of reverse movement. Stimulation of the posterior part of the nematode leads to the co-activation of both, forward- and backward-responsible circuits [2]. However, several internal mechanisms providing an intrinsic bias towards the higher activation of forward responsible neurons are identified. Eventually, inspired by the working principles of TW neural circuit, we design and implement a novel control module for an investor on stock market.

The work is structured as follows: Initially, state of the art researches on the C. elegans neuronal circuits are presented in Chapter 2. Goals, techniques and relevant results are described in order to support the investigation on C. elegans neural network. Relevant sources are then summarized and compared. Afterwards, in Chapter 3, we describe the models, procedures, techniques and tools which are utilized to perform the analysis on TW circuit. Moreover, methodology of designing the neural controller for the investor on the stock market is described in Chapter 3. Chapter 4 focuses on the detailed analysis of neurons and synapses of the TW circuit. At the end of this chapter, minimal TW circuit

is constructed and evaluated. Results of the analyzes are summarized in a short way. Chapter 5 describes the example of investor module driven by the C. elegans-inspired neural network. Eventually, we further discuss our results and indicate future research directions on the C. elegans NCs in Chapter 5. All the materials are provided in the *Appendix* section followed by the list of references.

CHAPTER 2

State of the art

This chapter covers the relevant literature sources to the investigation of C. elegans neural network and other related scientific activities. The goal is to analyze the current status of the research and build the background for the further research.

2.1 Biological sources

This section provides a references to the relevant research on the C. elegans neural network with dominating biological point of view.

The richest reference to the detailed physiological properties and anatomy of the nematode C. elegans can be found in WormAtlas [13]. It includes the wiring model of all neurons, description and references to the individual neurons, cell identification, genes expressions, etc. The responsible community of scientist keep track of the current state of the art and periodically updates the corresponding data. It is easy to find all relevant resources to each of the single neurons, which makes the analysis of the circuits and roles of the neurons easier. To simplify the work with complex structures, WormAtlas implements couple of interactive tools like WormWiring [14] for the synaptic connections, Slidable Worm [15] for the localizations of the muscles, organs systems and neurons and WormImgae [16] to display the worm of specific age, sex, tissue type, genotype.

WormWiring datasets can be further utilized in order to construct and analyze the entire neural network. neural circuit of the C. elegans nematode can be vertically divided into two parts – left and right. There are neurons present on the left and also on the right side (e.g. AVA neuron). To distinguish their localization, they are marked with -L or -R suffix. The remaining neurons (e.g. DVA neuron) are present only in one copy. Despite the fact, that the right side consists of the same neurons like the left side, they are asymmetric in term of number and directions of synapses. The neurons together with synaptic and electrical connections build the structure of the neural network in

the hierarchical modular way with weak inter-modular interaction [17]. The modules, inter- and intra-modular connections follows the fractal nature, which suggests a similar topology of the network no matter of the hierarchical level. The loose coupled modules are functionally independent units communicating through the few hubs with the rest of the network. The topology has been described using three topological parameters – probability of degree distribution, clustering coefficient and neighborhood connectivity. The smallest basis of the C. elegans network has been described as triangular object. It is supposed, that even the organisms with more complex neural network are based on the triangular motif but the hierarchy exhibits a larger number of levels [17].

Based on the functional classification, the neurons can be divided into three major groups – *sensor neurons*, *interneurons* and *motor neurons* [3, 4, 2, 5, 8]. Interneurons can be further classified into 3 classes - *primary*, *secondary* and *command interneurons* [5]. The *primary interneurons* are direct targets of the sensor neurons, *secondary interneurons* are the downstream neurons of the primary interneurons and together with primary interneurons provide synaptic output to the *command interneurons*. The command interneurons are supposed to control the locomotion in multiple biological activities like chemotaxis, thermotaxis, touch sensation and others. The functional mapping of classes of interneurons provides a promising assumption about the architecture of the biological neural controllers.

Vertical analysis of the C. elegans nervous system identify circuits, pathways or groups of neurons building the functional units within the network [5, 2, 8, 18]. For example, TW circuit, responsible for processing the tap and touch stimulus has been identified [2]. The classification of the neurons of TW circuit can be found on Figure 2.1 – sensor neurons (squares), interneurons (circles), motor neuron pools (triangles). The tap event is captured by a subset of the seven sensor neurons. The anterior sensor neurons ALM and AVM handle the touch in the anterior part of the worm body and initiate the backward locomotion. The posterior touch is governed by the PLM and PVD neurons causing the worm to move forward. Postsynaptic interneurons to the sensor neurons process the signal and command the motor neurons, which have a direct connections to the muscles. It is supposed that the AVB interneuron has a prominent role in controlling of the forward movement and the AVA interneuron has the majority in controlling of the backward locomotion [2].

One circuit of the C. elegans neural network can play different roles under specific strength of the stimulus. The relatively simple circuit, consisting of 5 neurons, has been selected in order to make a detailed description of the signal flow starting at sensor neuron and ending in motor neurons. Based on different strength of the stimulus applied to the ASH sensor neuron, the underlying circuit initiates or inhibits the backward locomotion. It proves that a polymodal sensor neuron can trigger different responses in term of nematode locomotion [8]. ASH is a polymodal sensor neuron sensitive to nose touch, hyperosmolarity and volatile repellent chemicals [19]. By stimulation of this neuron different behavioral responses can been triggered. Two partially independent sub-circuits – *disinhibory* and *stimulatory circuit* – has been identified. If the *disinhibory circuit* is

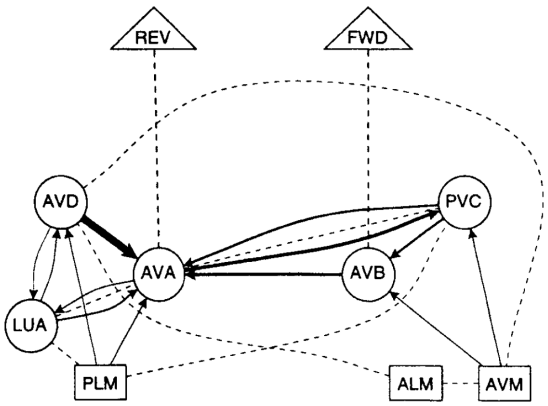

Figure 2.1: **Wiring model of C. elegans tap withdrawal circuit** [9]. The sensor neurons are depicted by the squares, interneurons by the circles and the motor neuron pools are simplified displayed by the triangles. The connections between the neurons are either chemical synapses (directed arrows) or gap junctions (dashed undirected lines). The number of connection corresponds to the width of the arrow/line.

activated, it inhibits the backward inhibition (which results into backward movement), the *stimulatory circuit* provide a direct support to the backward locomotion. The nose touch inhibits through the *disinhibory circuit* the backward inhibition and activates the *stimulatory circuit*, which supports the backward movement. Concluding this, both of the circuits, if they are activated, support backward locomotion. The hyperosmolarity stimulus is much stronger stimulus compared to the nose touch [8]. If the C. elegans would not escape from the highosmolarity environment, it may lead to its dead. To this end, the *disinhibory circuit* is inhibited, which on one side inhibits the backward initiation but on the other side disables the neck muscles, stopping the head oscillations. The *stimulatory circuit* is activated, promoting the backward locomotion and together with stopped head oscillations, supporting much more efficient escape compared to the nose touch. This behavior has been proven by functional imaging, optogenetic interrogation, genetic manipulation, laser ablation, and electrophysiology [8].

Multiple experiments to determine the polarities of the chemical synapses has been performed [2, 8, 3, 20, 21]. The synaptic polarities model is crucial to make assumptions which neurons are activated and which are inhibited during the processing of the stimulus. With the wiring model and polarities of the synapses, we are able to estimate the roles of the neurons and synapses. Starting with the simplified polarity model, where single neuron has only all synapses excitatory or all synapses inhibitory to all of its postsynaptic targets, the more complex polarity models, based on the probability of inhibitory nature of the neurons has been proposed [21]. One class of experiments investigate the polarities by the theoretical manipulation of synaptic conductance and gap junction conductance. The other class of experiments has been executed with the help of laser ablations, measuring the ability of C. elegans to move in the correct direction in response to the touch stimulus. The experiments has proven the hypothesis, that majority of the neurons

expose inhibitory synapses and therefore the gap junctions play crucial role in TW circuit [2, 3]. The issue of controlling the motor neurons by the inhibitory command neurons [2, 3, 20] has been addressed in [21]. The solution are the strong electrical couplings between the command interneurons and motor neurons. Therefore, despite a different configurations of synaptic polarities, C. elegans moves forward by default because of the forward responsible motor neurons receive a stronger input than the backward responsible neurons [22, 21]. Stimulating the backward responsible circuit, the corresponding motor neurons receive through the electrical synapses higher activation compared to the default activation of the forward motor neurons.

More complex polarities analysis has been performed by theoretical examination of the synaptic polarities validated with experimental data [21]. Theoretical experiments has been performed on the selected partial neural network with all possible polarity configurations by modulating the amplitude of the strong input and the excitation level of the ASH sensor neuron. Furthermore, "computer" ablations has been executed in order to construct the probabilistic model of being inhibitory for the neurons. These probability model is compared to the experimental data using the Euclid distance (ED). The experiments utilize laser ablations for ablating one to four neurons at once and express the change of time spent on each direction of locomotion. It has turned out, that almost all interneurons have a high probability of being inhibitory and only few have a bigger probability for firing an excitation signal [21]. Set of neurons having the prominent impact on the overall output of the circuit has been identified. Different activation levels of these neurons have a significant impact on the ED between the theoretical and empiric model.

Series of biological experiments has observed complex decision making procedures of C. elegans in specific situations [23]. The simplest decision *go* or *no-go* can be characterized as actions vs. inaction. The common scenario for such a decision is the escape reflex or withdrawal from the environment of hyperosmolarity [8]. In the scenario where one of the two possible behavioral actions to the same stimulus can be chosen, *behavioral competition* decision making is applied. The probability of approaching or avoidance given by gene expression and structure of the neural network is modified by the initial conditions of the experiment. The evidence of the bistable switch composed of several interneurons [3, 6] responsible for mutual inhibition of concurrent decisions has been confirmed by laser ablations [5]. Increasing the number of possible behavioral choices or the number of simultaneous stimuli leads to a more complex decision making, but still based on the proximal causes of selecting one of the alternatives [23]. Such a decision making can be assumed as *behavioral choice* [24] and together with the more complex *value based decision making*, which depends also on the ultimate causes, ensures the variability and reliability in the behavior of C. elegans.

Variability in the animal's behavior is an important feature supporting the evolution and adaptation of the organisms to the specific environment and keep the diversity among the individuals of the same specie [25, 26]. The evidence of variability of response of the C. elegans nematode has been discovered on the example with the odors [18]. If

the C. elegans is putted close to an attracting and repellent odors at the same time, behavioral choice based on the proximal causes is undertaken. During the experiment specific number of nematodes has been located close to the attracting odor on the plate. Not all of the animals were moving towards the attracting odor, there was a small number of worms not responding to the attraction. By measuring the calcium presence in the neurons, the variability and reliability responsible group of neurons has been observed. The current state of the motor neurons is integrated via feedback loops to the interneurons and plays an important role in decision making process [18, 7]. This recent hypothesis weakness the common understanding on the direction of signal processing, which is supposed to be top-down (from sensor neurons to motor neurons). Again, laser ablations has been utilized in order to examine the role of the neurons. The circuit responsible for the behavioral variability and reliability consists of three interconnected neurons – AIB, AVA, RIM. Two of them (RIM and AVA) support the variability and the third one (AIB) promotes the reliability of the worm's behavior. Depending on the combination of their internal state (ON/OFF) the variability or reliability is suppressed, which can be considered as probabilistic decision making procedure.

The next step in the neural network analysis is the mathematical modeling. Model allows to scale the computations to the specific part of the network and formulate the assumptions about the features of the circuits. The mathematical model for the TW circuit rely on the RC circuit [27] and computes the voltage potential of i-th neuron based on its physiological parameters and current flowing into and out of the neuron. The mathematical model describes the dynamics of the i-th neuron in the circuit including membrane leakage, external stimulus current, gap junction current and also the synaptic current. The change of the voltage potential during the time for a single neuron is defined by the followed equation [28]:

$$R_m C_m \frac{dV}{dt} = V_{LEAK} - V_i + R_m(I_{syn} + I_{gap} + I_{ext}) \tag{2.1}$$

where R_m stands for the membrane resistance, C_m for the membrane capacitance. V_{LEAK} describes the membrane leakage potential, V_i means membrane potential and sums of the incoming synaptic, electric and external currents are expressed by the I_{syn}, I_{gap}, I_{ext}, respectively. The voltage of the i-th neuron in the point of time depends on its physiological parameters (membrane capacitance and resistance), negatively on the potential leaked by the membrane and positively on the sums of incoming currents from the gap junctions, synapses and external environment. This model cannot be validated by the biological measurements because the current technology stack does not allow the global electrical measurements on the voltage activations of the neurons. To this end, calcium imaging technique is involved to supply the electrical measurements [11]. The calcium level inside the neuron can be interpreted in relation to the locomotion as a sign of activation or deactivation of the neuron during specific phase of the locomotion. As a result, it has been shown that behavioral motion sequences can be interpreted as a state diagram where the states represent the phases of locomotion and the transitions determines the possible sequences [7]. In the experimetns, C. elegans has been taken

away from he plate containing food supposing initiation of the local search strategy [7, 29]. Principal component analysis (PCA) of the brain-wide activity of 109 neurons by measuring the calcium level by fluorescence indicator has been performed. The activity diagram has revealed that the expression of the principal components encodes a sequence patterns of activations of neurons [7]. Capturing the calcium level of the large number of neurons in one experiment run, gives a advantage of understanding the global principles and activities behind the C. elegans neural circuit. For example, the activation of the RIM neuron (polymodal inter/motor neuron) has been at 90% connected with the initiation of backward locomotion. Furthermore, the functional opposite neurons (playing important role either for the forward or backward locomotion) expose an opposite signs of their principal component weight. Studying the patterns in the results from PCA, it has been discovered that the forward movement of the C. elegans can be decomposed into following actions: forward movement, slowing, backward movement, continue forward via dorsal turn, and continue forward via ventral turn. The sequence has been transformed into a state diagram where the states represent the phases of the forward locomotion and the unidirectional connections between the states describe the possible transitions between the phases.

One of the drawbacks of calcium imaging provide is an insufficient resolution to detect the rapid changes of the worm's behavioral states. Therefore the the results produced by calcium imaging has been extended by the measuring the velocity of the centroid of the C. elegans. The video analysis pointed out a very short phases of the locomotion where the worm's velocity decreased under 0.05 mm/sec. This observation has been marked as a pause in the movement. It has been observed mostly in cases, when C. elegans changes its crawling from forward to backward and the other way around. This knowledge has been used to transform the features of the neural network to the mathematical mode and develop the framework for simplifications and generalizations of the behavior, which could be tested and integrated to the similar controlling scenarios. The locomotory behavior can be expressed as flip-flop neural circuit with mutual inhibition of the opposite states. To this end, random search behavior [7, 30] has been addressed to the transformation to sate diagram. The local search strategy can be decomposed into four states – forward crawling, backward crawling and two pause states between the forward and backward and vice versa. Furthermore, the analysis of the transitions between the states of the C. elegans locomotion suggests, that the states are changing in a clockwise cycle. The probability of another direction of change are rapidly smaller [30].

2.2 Machine learning approaches

Overview of application of the C. elegans neural network in machine learning is contained within the following section. Most of the examples employ the neural network in controlling domain.

In the recent years, the anatomical data of the C. elegans has been transformed from the WormAtlas [13] to a artificial model called OpenWorm [31]. The goal of such a

transformation is to support future utilization of the biological controller in the computer science, especially in machine learning and controlling. Furthermore, simulating thousands of cells and interactions in the computer may lead to a global understanding of the processes inside the nematode. Another beneficial value of the computer simulations are the predictions on the the network capabilities, which can not be measured with the actual technology stack. Global theoretical experiments on the C. elegans neural network may extend the empirical experiments limited by the laboratory environment and equipment. Among the results of the well described digitalization process, we can find several useful tools like *DevoWorm* [32] focusing on developmental processes in C. elegans through data analysis, visualization, and simulation, *OpenWorm Browser* [33] allowing the users to interact the C. elegans anatomical model within a web browser, *NeuroML C. elegans Connectome* [34] providing virtual visualization of neurons and network, *Sibernetic* [35] simulating muscle tissues of C. elegans and *Geppetto* [36], which is a multi-platform web-based graphical interface allowing users to define own simulations of the neural network. Most of the tools are still under development and because they are not fully tested, they can only be utilized as a supportive material.

Several adoptions of the smaller or larger subsets of the C. elegans neural network has been developed [37, 38, 39]. Parameters describing the physiological properties of neurons and synapses has to be configured in order to simulate the C. elegans neural circuit within computer. Even, the biologists were able to measure some of the membrane parameters like membrane capacitance and resistance [2], there are still many neural-circuit-related parameters of unknown value and variance. The quantification of the circuit parameters is mostly powered by the optimization algorithms [38, 39]. In our recent work, we explored the varying parameters space with bounded-time reachability analysis of the underlying circuit [40]. We have estimated the probability of various neural circuit outputs related to parameter uncertainty. This technique helps to estimate the impact of laser ablations on the circuit response not yet performed by biologists. Furthermore, in most of the computer simulations [37, 38, 39] single compartment model of dendrites is used for the neurons, reducing the complexity of the non-linear integration of the incoming electrical currents [41]. Therefore, the computer simulations are adopting the behavior of C. elegans rather qualitatively than quantitatively. Despite the fact, that the simulations of copy-pasted C. elegans neural network have allowed the robots to intercept the anterior and posterior harsh or gentle touch, nose touch and the chemotaxis, there is still missing link to the explanation how the specific neural circuits process and evaluate the stimulus in order to command the motor neurons and how are the parallelism and concurrency principles implemented.

C. elegans neural network has been adopted to the motion controller of Lego Robot (EV3) [37]. The transformation of the nervous system to the robot's controller required some simplifications regarding the anatomical properties of the neurons and synapses. Each of the 300 neurons has been represented by a single process to allow the parallel data processing in the network. In the result, the robot has moved in the similar way as the C. elegans does, without the need for developing any additional logic for the motion

controller. In other words, copying the neurons and synapses with their exact structure, also the behavioral sequences encoded by such a network are copied.

Neural circuit controlling the gentle touch stimulus processing together with the kinematic model of the motor neurons generating the sinusoidal sequences of movement has been developed. Model of the neural network has been evolved with a real-coded genetic algorithm in order to find the satisfying configuration for the synaptic weights and the neurons characteristics [38]. The resulting artificial worm exposes qualitatively similar sensing and processing of the gentle touch stimulus to the real C. elegans individuals. The evolved model of the neural network parameters does not necessarily corresponds to the values of the biological network, as the evolution fits the overall output of the artificial model to the desired locomotory responses, so the internal controlling mechanisms are definitely not validated against each other. The outputs of both of the networks are similar. but the intrinsic logic may differ significantly.

Another machine learning technique to understand the principles of the biological neural network is the optimization by simulated annealing [42] used in global optimization processes in a large search space. This approach has been adopted in optimization of network candidates for the chemotaxis [39]. The complete (each neuron is connected bidirectional to all of the other neurons) neural circuit consisting of one sensor neuron, three interneurons and one pair of motor neurons controlling the dorsal and ventral muscles is supposed to control the attraction or avoidance to the chemicals. The synaptic current has been simplified to a linear function of the presynaptic voltage to provide a starting point for the future analysis of the non-linear networks. The advantage of linear network is easy utilization of rule extraction method leading to an identification of the dependencies between the defining parameters of the chemotaxis behavior [43].

More general approach to adopt the biological neural network into a controlling domain has been utilized to propose new computational paradigm called *Neural programming* (NP) for developing controllers for Cyber-Physical Systems (CPS) like cars, planes, smart houses has been proposed [44]. One of the major problems in the optimization process, which is a threshold value checking against the current value with the IF statement doing the optimization stepwise, has been identified. Getting closer the threshold value, the function says YES, and right after the threshold value, the function returns NO. However, in the real world scenarios, there is not such a sharp threshold for a good solution. To avoid a threshold checking, smooth decision model based on random variables (RVs), which are mutually dependent Gaussians, has been constructed. The model utilizes several new statements, like *NIF* and *NWHILE* as a neural correspondence to the IF and WHILE directives.

The execution of the *NIF* statement is illustrated on the following example [44]:

Listing 2.1: Neuronal IF statement.

```
nif (x >= a, σ²) S1 else S2
```

The procedure follows two steps: (i) Find an confidence interval I that a $S1$ is executed.To find the desired interval I, we compute the difference between the a and x. A larger value for this difference means a higher value of probability, that $S1$ will be executed. (ii)For the random sample from a Gaussian distribution (GD) $\mathcal{N}(0, \sigma^2)$, check if it falls into I. If yes, the $S1$ branch is executed, otherwise the $S2$ is executed. For the $\sigma = 0$ the program compute no uncertainty and the *NIF* behaves like a common *IF* statement.

As a demonstration of the NP computational model, solution to the real world scenario has been provided [44]: parallel parking of the robot controlled by the C. elegans connectome. The membrane potential has been mapped to the distance of the robot to the parking place, retrieved from the sensors in the Equation 2.1. The circuit has commanded the wheels velocity and the turning angle in order to perform a correct parallel parking. By the few additional mathematical adjustments, the C. elegans inspired neural controller has been constructed, supporting a smooth optimization process based on NP, enabling the robot to perform a correct parking from the different initial positions.

Literature summary

This section provides a short summary of the related biological and technological sources in order to identify the interceptions and differences of the corresponding results.

Regarding the neural structure discovery, there are small differences in numbers of the synapses and gap junctions in the older [4, 2, 5] and more recent researches [30, 18, 45]. Also the probabilities of being inhibitory for the chemical synapses differs according to the technique used for determining the polarities [2, 21]. It has been assumed, that one neuron can either have all outgoing synapses excitatory or inhibitory [4, 2]. The increased capabilities of the measuring devices and the laser microsurgery has shown that one neuron can connect to its postsynaptic targets with both, excitatory and inhibitory synapse [21, 46]. The investigation on the synaptic polarities model is one of the challenges to understand the signal processing within the neural network. It is assumed, that the new optogenetic devices capable of global wide resolution of neurons voltage levels shed more light into the identification of activated/inhibited sub-circuits building a functional blocks in the signal processing procedure.

Further, there is an open question on the direction of the signal processing. While the older researches [5, 8] assumed only the feed-forward signal propagation from the sensor neurons to the interneurons and finally to the motor neurons, the recent studies has confirmed the feedback integration of the state of motor neurons to the interneurons with a significant impact on the decision making. On the other hand, there is a wide agreement on the responsible command interneurons controlling the forward (AVB) and backward (AVA) direction of movement despite the fact, that the laser ablation of these prominent interneuorns only decreases the ability of the movement controlling but they did not disable it [21].

Application of the machine learning techniques for the modeling and simulating the biological neural network requires a specific level of reducing the physiological complexity

of the neurons and synapses [37, 38, 39]. The reduced model has to be optimized in term of network parameters resulting in qualitatively similar behavior to the real network, but because of artificial optimization of the synaptic weights and neuron characteristics, the controlling mechanism of the artificial worm may differ to the real C. elegans. Another challenge of the reusing the biological neural networks in the robot controlling domain is the mapping of the input current to the different physical units like distance, velocity [44].

CHAPTER 3

Methodology

This chapter provides an overview of models, procedures, techniques and tools utilized to perform the analysis of TW circuit. Furthermore, the methodology of constructing the neural controller for the investor on the stock market is contained within this chapter. The analysis of TW circuit is divided into modelling, experimenting and evaluation phase.

3.1 Modelling

To perform the theoretical experiments on TW circuit, the NC has to be modelled in the computer using appropriate data structures, readable by the programming language. The starting point of the modelling the NC is the connectivity diagram, which indicates how the neurons are interconnected, what kind of synapses they build and what the polarities of the chemical synapses are. To this end, biological references contained within WormAtlas [13], WormWeb [47] and the interactive online tool *Synaptic Connectivity of C. elegans* [45] are utilized in order to establish the connectivity diagram of the neural network. There are small inconsistencies in the number of connections between the sources. The first measurements on pharynx neuronal wiring has been done in 1976 by Albertson & Thomson [48], continued with whole neuronal network wiring model by White et al. in 1986 [4] and followed by research of Chklovskii group in 2006 [49]. In our modelling, we use Chklovskii data, slightly modified by the OpenWorm community in 2013 (personal communication) 3.1C. There is still open question how to model monadic (one origin, one target) 3.1A and polyadic (one origin, multiple targets) synapses 3.1B, since there is no related research on the weights of these connections. Furthermore, recent study [50] pointed out, that presence of electron microscope derived synapses does not determine for 100% if the connected neurons really impacts each other or not.

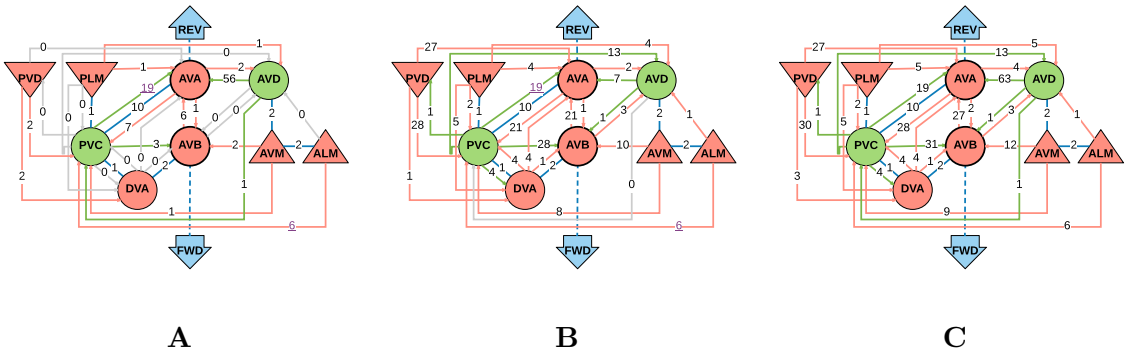

Figure 3.1: **Wiring models of TW circuit composed of monadic and polyadic synapses.** (A-C) The four sensor neurons are represented by the triangles, interneurons are depicted by the circles, command interneurons AVA and AVB are displayed with the strong borders. The excitatory interneurons and their outgoing synapses are filled with the green color, inhibitory interneurons and their synapses with the red color. The blue connections represent the gap junctions. Underlined violet synapses indicates that there is missing knowledge on the portions of monadic and polyadic synapses. Therefore, they are counted in monadic and also polyadic model. Blue arrow objects represent the corresponding group of motor neurons responsible for forward/backward movement. (A) TW circuit containing only the monadic chemical synapses. (B) TW circuit containing only the polyadic chemical synapses. (C) TW circuit containing both, monadic and polyadic chemical synapses.

The polarities of the chemical synapses has been derived from the probabilistic models [2, 21, 8] indicating the probability of the neuron to have an inhibitory impact on its postsynaptic targets. In the analyses, the simplified polarity model is adopted [2] – a single neuron express either excitatory or inhibitory synapses to all of its postsynaptic neighbors. More recent studies [21, 46] suggest the possibility of one neuron to connect its targets with both, excitatory and inhibitory synapses. There are several tools available to create a model of the neural network or just interact existing model. The OpenWorm community [31] published several helpful programs and libraries dedicated to C. elegans neural network. The newest open-source web browser application *Geppetto* [36] visualizes the complete biological model of C.elegans. It supports selective points of view for displaying muscles and neural network. Thanks to the modular architecture of *Geppetto*, user can experiment the specific part of the neural network from the console, one can define own experiments, store and plot the data. Neural network of different genders or mutants of C. elegans or even different organisms can be uploaded, because of support the common used data format for the neural networks. It is possible to install additional widgets to achieve more customizable and detailed opportunities for experimenting a specific model. However, the current version of Geppetto application does not implement all planned features in an efficient way, some of the features are not fully tested, which results in a huge amount of consumed time for even small experiments. The available pre-version serves as an example what will be available soon (personal conversation). Another 3D anatomical atlas of C. elegans – *WormBase* [51] – has been transformed into

NeuroML (A Model Description Language for Computational Neuroscience) model, which could be afterwards directly passed to the *neuroConstruct* [52]. The final software is called *CElegansNeuroML* [53]. *neuroConstruct* is a Java tool supporting the construction of neuronal networks models capable of simulating a lot of biological features. Besides others, the tool considers a realistic cell morphology with the 3D position in the network, voltage-gated and ligand-gated ion channels and synaptic connectivity. It even allows to the import the realistic biophysical cell mechanisms like channels. The models can be further simulated on NEURON, GENESIS, MOOSE, PSICS and PyNN platforms [52]. As an upgrade to the *CElegansNeuroML*, there is also one new initiative called *c302* [34], which is still in under construction. The current version utilizes the *NeuroML2* format to encode the C. elegans connectome. Using the *jNeuroML GUI* it is possible to print out the voltage traces or calcium level inside of selected set of neurons. User is able to change the scale of details to focus on specific components of the C. elegans body.

In order to model the TW circuit consisting of a subset of neurons presented in [2], we use a matlab abstraction developed as part of the work on *neuronal programming* [44]. The dynamics of the circuit is modeled by the mathematical model presented in [28]. The following Listing 3.1 describes the computation of the membrane potential of the i-th neuron using the matlab built-in nonlinear ODE *ode*45 simulation function. The wiring diagrams for chemical synapses and gap junctions are contained in the *W_gap* and *W_syn* matrices, respectively. V is the vector of the presynaptic neurons membrane potentials and $V(i)$ represents the membrane potential of the postsynaptic neuron. The source computes the Equations 3.1 - 3.4, which are derived from the Equation 2.1. The electrical current passing through the gap junction between the presynaptic neuron j and the postsynaptic neuron j (Eq. 3.2), $I_{gap}^{(ij)}$ is computed as a product of the gap junction conductance $g_{gap}^{(ij)}$, the weight (number of gaps) of the gap junctions $w_{gap}^{(ij)}$ and the difference of the voltage potentials between the presynaptic and the postsynaptic neurons. The current of a chemical synapse (Eq. 3.3) is a product of the weight of the chemical synapse (number of synapses) $w_{syn}^{(ij)}$, synaptic conductance $g_{syn}^{(ij)}$, and the difference between the reverse potential of the synapse $E^{(ij)}$ and the postsynaptic neuron voltage level $V^{(j)}$. The synaptic conductance (Eq. 3.4) is computed as a quotient of maximal synaptic conductance $\bar{g}_{syn}$ and the expression dependent on presynaptic current V^j, presynaptic equilibrium potential V_{EQj} and presynaptic potential range V_{RANGE}.

$$\frac{dV^{(i)}}{dt} = \frac{V_{Leak} - V^{(i)}}{R_m^{(i)} C_m^{(i)}} + \frac{\sum_{j=1}^{N} (I_{syn}^{(ij)} + I_{gap}^{(ij)}) + I_{stim}^{(i)}}{C_m^{(i)}} \tag{3.1}$$

$$I_{gap}^{(ij)} = w_{gap}^{(ij)} g_{gap}^{(ij)} (V_j - V_i) \tag{3.2}$$

$$I_{syn}^{(ij)} = w_{syn}^{(ij)} g_{syn}^{(ij)} (V^{(i)})(E^{(ij)} - V^{(j)}) \tag{3.3}$$

$$g_{syn}^{(ij)}(V^j) = \frac{\bar{g}_{syn}}{1 + e^{K(\frac{V^j - V_{EQj}}{V_{RANGE}})}} \tag{3.4}$$

Listing 3.1: Computation of i-th neuron's voltage level in Matlab

```
function [Vprime] = TWModel_dynamics(time, Voltage)
Leakage_potential = -0.035;
Gap_junction_conductance = 5e-9;
Synaptic_conductance = 6e-10;
Presynaptic_voltage_range = 0.035;
K=-4.3944;

for i=1:length(neurons)
        % Stimulus current
        I_stim = IStim(i,round(t/dt)+1);

        % Leak current
        I_leak = (V_leak-V(i))/Membrane_resistance(i);

        % Gap junction current
        I_gap = Gap_junction_conductance*W_gap(i,:)*(V-V(i))
           ;

        % Synaptic current
        g = Synaptic_conductance./
            (1+exp(K*(V-Presynaptic_equilibrium_potential)/
            Presynaptic_voltage_range));

        I_syn = W_syn(i,:)*(g.*(Reverse_potential-V(i)));

        % f function
        Vprime(i,1) = (I_leak+I_gap+I_syn+I_stim)/
           Membrane_capacitance(i);
end
```

Based on the integral of depolarization difference between the forward responsible command interneuron AVB and the backward driving interneuron AVA, the direction of the locomotion is computed (Eq. 3.5). This number could not be interpreted as a response magnitude, it only specifies the relative proportion between the activation of neurons AVA and AVB to the behavior magnitude [2].

$$D = \int_{t_s}^{t_e} (V_{AVB} - V_{AVA})dt \begin{cases} D \geq 0 \rightarrow forward \\ D < 0 \rightarrow backward \end{cases} \tag{3.5}$$

D is proportional magnitude of the TW output. It represents the direction of the worm's crawling during the stimulation starting at t_s and ending at t_e. Positive D value implies the forward locomotion, negative D value represents the backward movement. V_{AVB} and V_{AVA} stand for membrane potentials of the AVB and AVA neurons during the stimulus episode, respectively. If D equals to 0, we simply assign this case to the forward locomotion, as this a default direction of the C. elegans locomotion.

3.2 Experiments

The experiments performed on the TW NC follow three different perspectives – (i) analysis of the synapses and neurons with respect to the anterior tap stimulus, minimal backward-responsible circuit is constructed (ii) analysis of the synapses and neurons when the posterior tap stimulus is applied, the minimal forward-responsible NC is constructed and (iii) analysis of the TW circuit, constructed by merging previous two minimal circuits, with respect to processing both, anterior and posterior taps. The analyses are based on the TW circuit model (Fig. 4.3).

The goal of the experiments is to measure the activities of the neurons in order to make the assumptions about the grouping of the neurons into functional sub-circuits, doing one simple task of the overall locomotory activity. Moreover, we want to identify the simple neuronal pathways from sensor neurons to motor neurons to understand the procedures of signal processing and evaluating into controlling command to motor neurons. Here, we employ the stepwise "computer" ablation (the neurons and synapses are ablated one by one) on synapses and neurons of TW circuit to reverse engineer the roles of the neurons and synapses. The "computer" ablation is an artificial alternative to laser microsurgery on C. elegans, where neurons and even single synaptic connections without apparent injury to the axon may be ablated [54, 55]. The impact of the ablations is computed by the change of time spent on expected direction of locomotion 3.6 and 3.7. The change of time spent on forward locomotion δ_t^F is expressed as the difference of times spent on forward movement by the TW circuit without t_{TW}^F and TW circuit with ablation $t_{TW'}^F$. The same procedure has been used for calculating the difference in reverse movement δ_t^F. The largest δ_t^F and δ_t^R identify the essential neurons, synapses and gap junctions for initiating forward acceleration and backward crawling.

$$\delta_t^F = t_{TW}^F - t_{TW'}^F \tag{3.6}$$

$$\delta_t^R = t_{TW}^R - t_{TW'}^R \tag{3.7}$$

C. elegans default direction of movement

Forward locomotion is the default direction of C. elegans movement [56, 22, 21]. Researchers slightly differs in the reasons providing the intrinsic bias towards the forward locomotion [22, 21]. For purposes of our experiments we assume, that in the steady state (before and after the stimulus event) the AVB activation should be over the AVA activation. Concluding this fact, membrane potential of AVB should be greater than membrane potential of AVA during the entire simulation run. Impact of the tap default forward locomotion to our laser ablation experiments is that even we disturb the pathways of the posterior stimulus signaling from the PLM sensor neuron to the interneurons, C. elegans still moves forward. Only more invasive ablations could lead to the disabling of the forward locomotion.

3.2.1 Simulation details

The physiological membrane and synapses parameters are adopted from the Wicks model [2]. The simulation duration was set to $80ms$. One simulation step stands for $0.0001ms$. The stimulus current of $5e-10A$ is applied at the time $10ms$ and its duration is $30ms$.

The resting potentials for the neurons has been determined by simulation of TW circuit without any stimulus. After some time, the neurons reach their steady state, which is considered as initial state in our simulations Table 3.1 The values of resting potentials are in Volts.

Table 3.1: Resting potentials of TW neurons. The values are in Volts (V).

AVM	ALM	PLM	AVD	AVA	PVC	AVB	PVD	DVA
-0.0235	-0.0235	-0.0334	-0.0234	-0.0275	-0.0334	-0.0206	-0.0094	-0.0265

3.2.2 Time analysis

We compute the time spent by the worm on forward and backward locomotion with applying minor modifications to the TW Matlab model [44]. During the "computer" ablations, in each run of the program, one electrical or chemical synapse is knocked out and the circuit output is stored in the CSV file to allow easy and quick processing of results for further analysis. The amount of time spent on backward locomotion equals to number of milliseconds, when the Equation 3.5 holds a negative value for D. Furthermore, we are able to measure the voltage potential of neurons by Equation 2.1. In particular, we collect the voltage traces for command interneurons AVB and AVA and compare them element-wise after the simulation is over (Listing 3.2). The time spent on the forward movement is stored in the *forward* variable and time for backward movement in the *backward* variable.

Listing 3.2: Computation of time spent on forward and backward locomotion in Matlab.

```
for i=1:length(output_avb)
    if output_avb(i) >= output_ava(i)
        forward = forward + 1;
    else
        backward = backward + 1;
    end
end
```

3.2.3 Voltage traces analysis

Synaptic ablations modify the signal precessing within neurons and therefore impact the overall output of the TW circuit. Some of the impacts of synaptic ablations are invisible from the point of time spent on each direction of locomotion. Also the results of time analysis can be detailed explained by investigating on membrane potentials of related neurons. Therefore we apply a voltage traces analysis to deepen the understanding of what is happening inside of neurons during the synaptic ablations.

3.2.4 Building minimal backward- and forward-responsible circuits

In this section, we build minimal backward- and forward-responsible TW circuits. We list the steps where adding chemical or electrical synapse modify the overall result of the circuit in favour of promoting corresponding direction of locomotion as a response to the tap stimulus. We evaluate models based on their ability to recognize the tap stimulus and ability of supporting the default forward crawling during the steady state – before and after the stimulus – as well as variations on the levels of activation or deactivation of the AVB and AVA command interneurons in comparison to the membrane potentials within the TW circuit.

3.2.5 Neurons ablations

In the neuronal ablation experiments we cover the impact of neuronal ablation on the overall circuit output. We ablate only one neuron in each run of the program. In our experiments, we do not ablate sensory neurons, responsible for intercepting the tested tap stimulus and the command interneurons, responsible to command the motor neurons. Theoretically, the ablation of neuron is equal to ablation of all electrical and chemical synapses connected in any direction to such neuron.

3.3 Evaluation

The results of the experiments on the withdrawal behavior are compared and interpreted in order to assign the functional properties to the specific structural units of the neural circuit. The changes of time spent on each direction of movement after applying the “computer” ablation are compared to the membrane potential analysis of the neurons to

correlate the results of these two analyses. After the correlation process, the assumed functional mapping of neurons and synapses, obtained by performing the ablations is validated in respect to the biological measurements of the impact of laser ablations.

3.4 Demonstration

The extracted principles of the C. elegans NC are applied to the implementation of a simple investor decision module for stock market. The stock market environment is provided by the *Plus500* online platform, which a leading product on the field of Contracts for Difference (CFD's) [57]. It allows to trade shares, commodities, forex, etc. in the real stock market environment. Based on the values of the specific market indicators, investor decides on taking the position. Either, he buys shares or he shorts (sell) them. To save the time on integration of the C. elegans-based decision module into online application, the indicator values are generated by the program and used as an input to the investor module. The decision making part of the investor is a distributed neural controller constructed on similar principles as locomotory NC of C. elegans. It is developed as an console application in Matlab programming language taking the values of the indicator as an input and deciding on taking position on the stock market – SELL or BUY.

CHAPTER 4

Results

In this chapter a detailed overview of the achieved results is provided. We explain the purpose of each synaptic connection within the nervous system and generate the control principles existing within the TW neural circuit.

4.1 Anterior tap reflex

Anterior tap stimulus is applied to the sensory neurons and a backward locomotion is expected. we initially analyze the time and potential changes of ablated TW circuit compared to the complete circuit. We then, construct the backward-responsible minimal circuit from scratch.

4.1.1 Backward time period analysis

As long as we expect the worm to move backward as a response to the AVM tap stimulus, we are only focused on the time difference corresponding to the backward crawling. The following tables Table 4.1 and Table 4.2 indicate the chemical and electrical synapses ablations, which have the most significant impact on the time spent on backward movement after application of the tap stimulus to AVM sensor neuron.

The R_{NA} represents the time of reverse movement controlled by the TW circuit without any ablation. First two columns specify the localization of the chemical synapses in terms of presynaptic and postsynaptic neurons. N value represents the number of synapses, e.g. 13/63 means, the number of synapse is reduced from 63 to 13 during simulation, which corresponds to 50 ablated synapses. Finally, δ_{REV} is the time change spent on reverse movement if the specific number of synapses is ablated.

Table 4.1 points out three key synapses for emulating the correct processing of anterior tap stimulus. The AVA command interneuron is activated through the excitatory synapses

Table 4.1: Most important chemical synapses for the initiation of the backward locomotion.

$\mathbf{R_{NA}}$ **= 350 ms**			
Ablated chemical synapse			
From	**To**	**N**	$\delta_{\mathbf{REV}}$
AVD	AVA	0/63..51/63	-100%
AVM	AVB	0/12..9/12	-100%
PVC	AVA	0/19..2/19	-100%
PVC	AVA	3/19	-59.37%

from AVD. At the same time, the AVB command interneuron is deactivated by the inhibitory synapses from AVM. This behavioral *flip-flop switch*, where opposite behavioral choices are mutually inhibited, is necessary mechanism in order to allow the expected behavioral output to outperform the opposite behavior output. The PVC-AVA synapse has no direct impact on the activation of AVA or deactivation of AVB, but it has a positive impact on AVA in the steady state. If this synapse is missing, the state state membrane potential of AVA has a lower voltage so that the AVA activation can not outperform AVB inhibition during the stimulation of AVM.

Table 4.2: Most important electrical synapses for the initiation of backward locomotion.

$\mathbf{R_{NA}}$ **= 396 ms**			
Ablated electrical synapse			
From	**To**	**N**	$\delta_{\mathbf{REV}}$
AVM	AVD	0/2	-100%
AVB	DVA	0/2	-100%

The time analysis of the gap junctions proves the assumption, that sensor neurons express inhibitory synapses to their targets and the signal is passed through the gap junction to enable quick escape response [2]. We note that due to the absence of a gap junction from the second anterior tap sensor neuron – ALM – to AVD, the signal is passed to the AVM first, and then, reusing the same signal pathway as by the AVM tap stimulus, to the

AVD neuron. As a result, the ALM-AVM and AVM-AVD gap junctions are considered to be critical in order to pass the anterior tap stimulus to the layer of interneurons. The second critical electrical connection are the AVB-DVA gap junctions. These are part of the gap junctions pathway between the two command interneurons AVA and AVB Figure 4.1. Underlying gap junctions synchronize the membrane potentials of all involved neurons, which are: AVA, PVC, DVA and AVB. Specifically, the AVB-DVA gap junctions decrease the difference between the AVA and AVB membrane potentials. In case they are disconnected, the AVA activation is not able to win over the AVB deactivation.

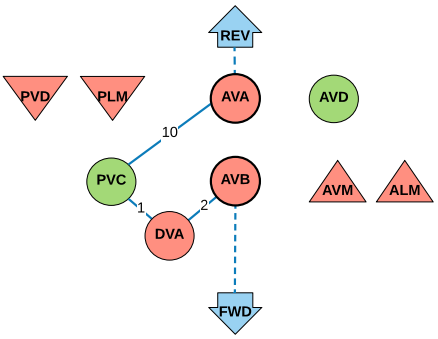

Figure 4.1: **AVA-AVB gap junctions pathway.** Membrane potentials of AVA, PVC, DVA and AVB neurons are synchronized across TW circuit in order to correlate command neurons AVA and AVB.

Following figures (Figures 4.2A-C) show the chemical synapses 4.2A and gap junctions 4.2B, which have a predominate impact on the initiation of the reverse movement, during the AVM tap stimulation. Figure 4.2C merges the important synapses and gap junctions together and provides a connectivity skeleton for the processing of anterior tap. The signal is propagated from the AVM sensor via gap junction to the layer of interneurons where the decision on direction of the locomotion is made and transferred to the command neurons. The PVC-AVA and AVB-DVA connections are not directly connected to the main processing pathway. They are supposed to regulate the correlation between AVA and AVB when no stimulus is applied. Note that this simplified circuit can not override the complete TW circuit, not even for the correct processing of the AVM stimulus.

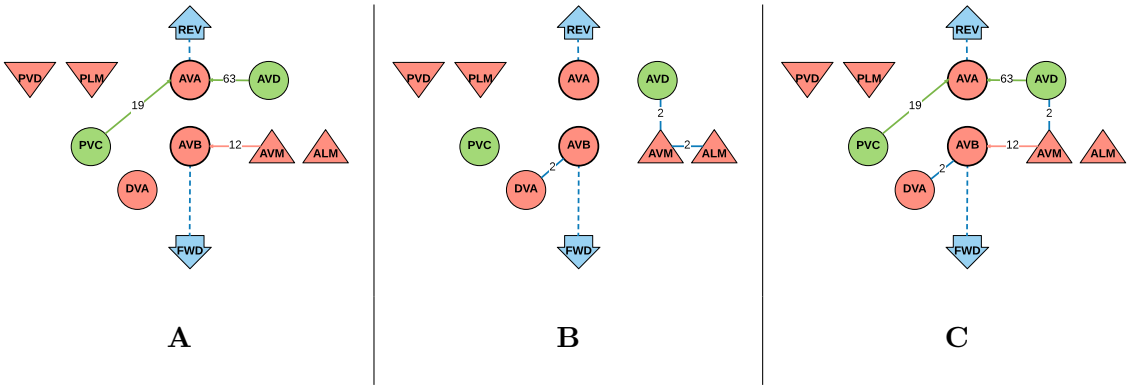

Figure 4.2: **Most important chemical and electrical synapses in TW circuit for the backward locomotion assessed by time analysis. (A)** The chemical synapses with the crucial impact to the backward movement.**(B)** The gap junctions building the important signal pathways for signal propagation from the sensor neurons to the interneurons.**(C)** Merge of synapses from (A) and gap junctions from (B) build a necessary skeleton for correct processing of anterior tap stimulus.

The key outputs from the above analysis are (i) the evidence of reusing one signal pathway for two different sensor neurons, (ii) *flip-flop switch* and (iii) synchronization pathway connecting AVA and AVB neurons.

4.1.2 Voltage traces analysis

If we apply tap stimulus to the AVM sensor neuron in the complete TW circuit (without any synaptic or neuronal ablation) we get the following voltage levels for AVB and AVA (Figure 4.3).

Time analysis pointed out crucial chemical synapses and gap junctions for correct process and evaluation of the anterior tap stimulus. One of these are 63 synapses between AVD and AVA neurons. Cutting off these synapses,one by one, leads to gradual decreasing of the ability of the C. elegans to respond to the AVM tap stimulus (Figures 4.4A, 4.4B). In particular, knocking out at least 12 of 63 synapses leads to a complete lost of backward response to the anterior tap. It is also observable, that AVA activation is proportional to the number of incoming connections from AVD, while the AVB inhibition does not change by ablating AVD-AVA synapses. The dependency coefficient of AVA activation on the number of synapses from AVD can be derived from the Equations 3.1 where the synaptic current depends on the weight (number of) of the incoming synapses (Equation 3.3). Ablation of 12 synapses decreases the AVA membrane potential in average at -1.87 mV. For the average change of the membrane potential, we use an equation 4.1, where T holds for the simulation duration, $V^{'}$ is the voltage of the respective neuron in the ablated TW circuit and V^{NA} is the membrane potential of respective neuron in the full TW circuit.

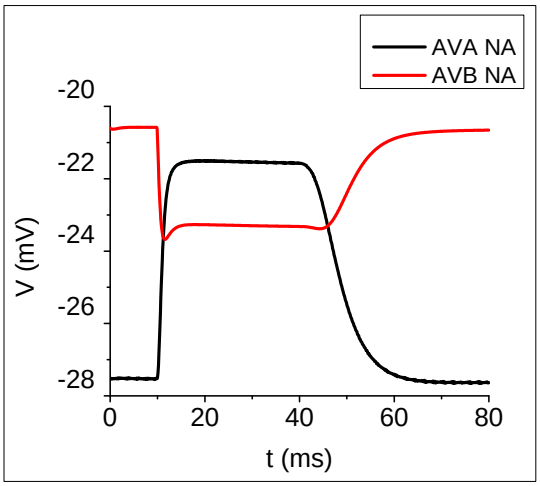

Figure 4.3: **Voltage levels for AVB (red) and AVA (black) neurons during the anterior tap stimulus.** *NA* suffix indicates, that no ablation is applied to the TW circuit.

Similarly, if the PVC-AVA excitatory synapse is reduced from 19 to 2 connections, the C. elegans can not respond with the backward locomotion. Again, the impacted neuron is only AVA, the change is -2.16 mV. This synapse does not play important role in signal propagating, but it modulates the membrane potential of AVA before and after the tap stimulus.

$$diff = \frac{\sum_{i=1}^{T}(V'_{AVA}(t_i) - V^{NA}_{AVA}(t_i))}{i} \tag{4.1}$$

Potential analysis for the AVM-AVB inhibitory synapse reveals the dependency of AVB inhibition on the number of AVM-AVB synapses, while the AVA remains activated at the same potential level (Figures 4.4C, 4.4D). 10 out of 12 chemical synapses are the minimal precondition on AVM-AVB connection to keep the worm respond correctly to the AVM tap stimulus. The change of AVB membrane potential is computed by the Equation 4.1 and is equal to +1.61 mV.

If the ablation of AVD-AVA synapses is combined with the ablation of AVM-AVB synapses and ablation of PVC-AVA synapses (Figure 4.4E) the effects of these three ablations are summed up, so that the AVA neuron receives at -4.38 mV weaker activation and AVB command interneuron receives a smaller inhibition about +1.38 mV. These changes in membrane potentials are equal to the changes in previous experiments, but they are summed together in this case. The worm completely loose the ability to respond with reverse movement to the anterior tap stimulus. It is important to remark, that the described three ablations behave additively, when they are combined together. Such an observation implies the fact that they do not interference each other in the TW circuit. Therefore, it is impossible to supply one of these synapse by adjusting the configuration of the other synapse.

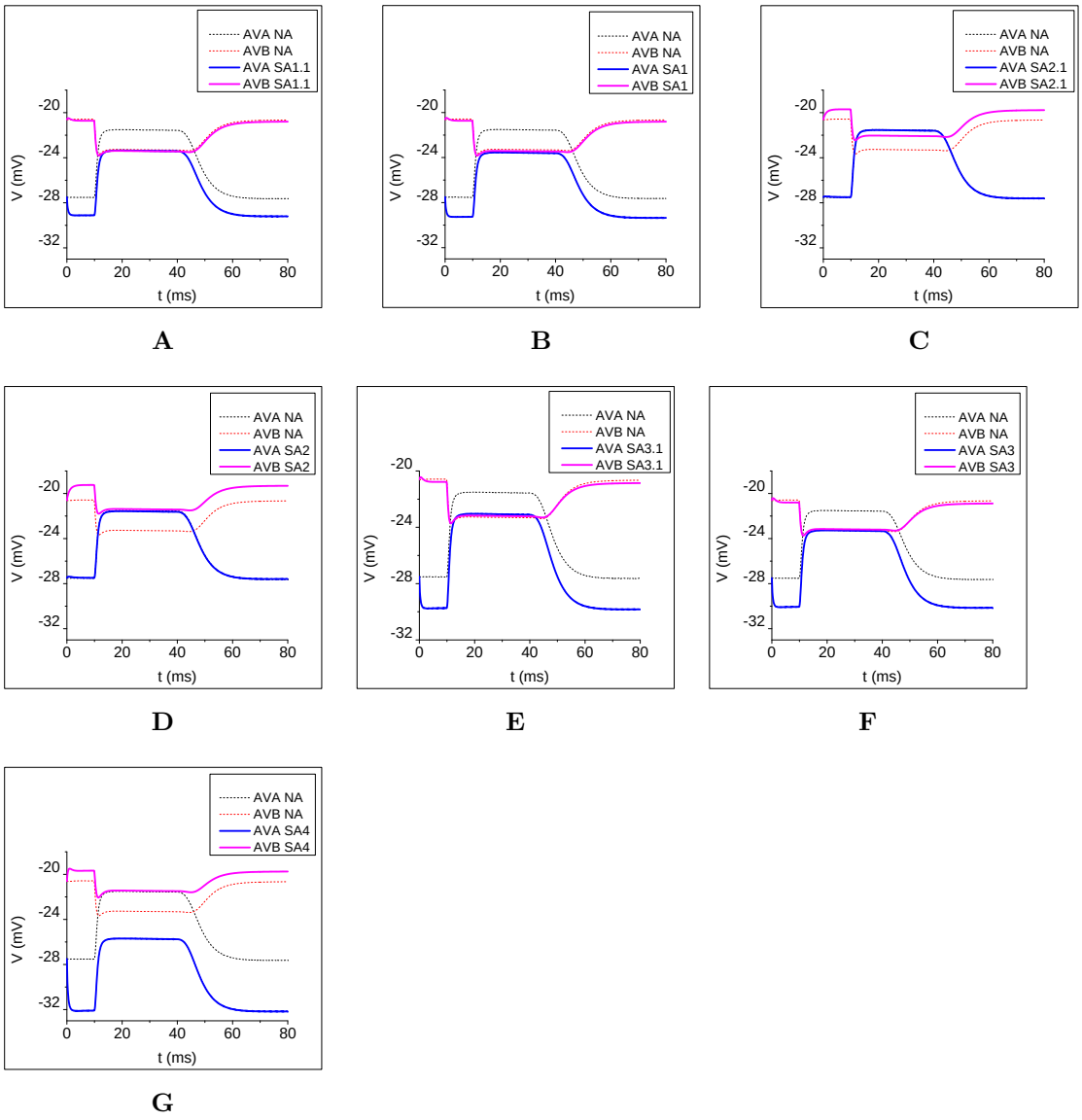

Figure 4.4: (Continued on the next page.)

Figure 4.4: **(Previous page) Reducing the number of chemical synapses for most important connections of backward-responsible circuit. (A-G)** The AVA and AVB voltage levels of complete TW circuit are displayed by the black (AVA NA) and the red (AVB NA) dashed lines, respectively. **(A)** The minimal number of AVD-AVA synapses, when C. elegans still responds with the reverse movement to the AVM stimulation. By the almost same deactivation of AVB interneuron, the excitation of the AVA interneuron is significant lower, because of AVD-AVA synapse is supposed to be excitatory. SA1.1 represents AVD-AVA synapses reduced from 63 to 52. **(B)** The number of AVD-AVA synapses is reduced from 63 to 51 synapses. In this case, the AVA activation does not outperform the AVB deactivation – the worm is unable to respond to the AVM tap stimulus with the backward movement. SA1 represents AVD-AVA synapses reduced from 63 to 51. **(C)** 10 synapses out of 12 is the minimal condition to AVM-AVB inhibitory synapse to keep the correct behavior of the worm when anterior tap applied. SA2.1 represents AVM-AVB synapses reduced from 12 to 10. **(D)** The number of AVM-AVB synapses is reduced to the 9 synapses. In this case the worm could not crawl backwards as a response to the anterior tap, because of AVB deactivation is not strong enough to allow the AVA outperform AVB. SA2 represents AVM-AVB synapses reduced from 12 to 9. **(E)** PVC-AVB synapse can be reduced to 4 connections to still support correct backward withdrawal. SA3.1 represents PVC-AVA synapses reduced from 19 to 4. **(F)** If the number of PVC-AVB synapses is lower than 4, the AVA membrane potential before and after the stimulus is lower, so that during the tap stimulus, AVA activation is not higher than AVB inhibition. SA3 represents PVC-AVA synapses reduced from 19 to 2. **(G)** Combination of the synaptic ablations from the B, D and F behaves additively in the overall result. The lower excitation of AVA from the B and F combines with the lower inhibition of AVB from the D. These two impacts are summed together into heavy disablement of the reverse locomotion. SA4 represents combinations of three ablations from B, D and F.

Potential traces analysis of the most important gap junctions from the time analysis (Section 4.1.1) helps to understand the role of the AVB-DVA gap junctions within the AVA-PVC-DVA-AVB gap junctions pathway. In the complete TW circuit, during the AVM tap stimulus, PVC interneuron is slightly activated because of the shared activation from AVA neuron through strong electrical coupling. The PVC activation is further passed to the DVA neuron, but at the same time, DVA neuron receives an inhibition from AVB command interneuron. Since there are two gap junctions from AVB to DVA, the inhibition from AVB is stronger than only one gap junction from PVC to DVA. As a result, DVA neuron is inhibited during the tap stimulus event and therefore it supports the AVB inhibition. DVA neuron is inhibited also before and after the stimulation, so it certainly has an inhibitory effect on AVB. If the electrical coupling between AVB and DVA is disrupted, the AVB membrane potential has a higher activation during the steady state, because it does not get inhibited by DVA. Therefore, also during the AVM stimulation, the AVB membrane potential is shifted to the higher values compared to the complete TW circuit. The AVA excitation is no longer able to win over AVB membrane potential.

The role of AVM-AVD gap junctions is more straightforward to understood compared to the AVB-DVA gap junctions. The circuit without such connection is not able to pass the tap stimulus signal from AVM sensor neuron to the interneurons and correspondingly cannot activate the correct command interneuron. This connection is necessary in order

to process ALM tap stimulus, which is second anterior tap-sensitive neuron. In the TW circuit, this neuron is missing gap junctions to the layer of interneurons and to forward the stimulus signal, it utilizes the AVM sensor as facilitator of gap junctions pathway to AVD neuron.

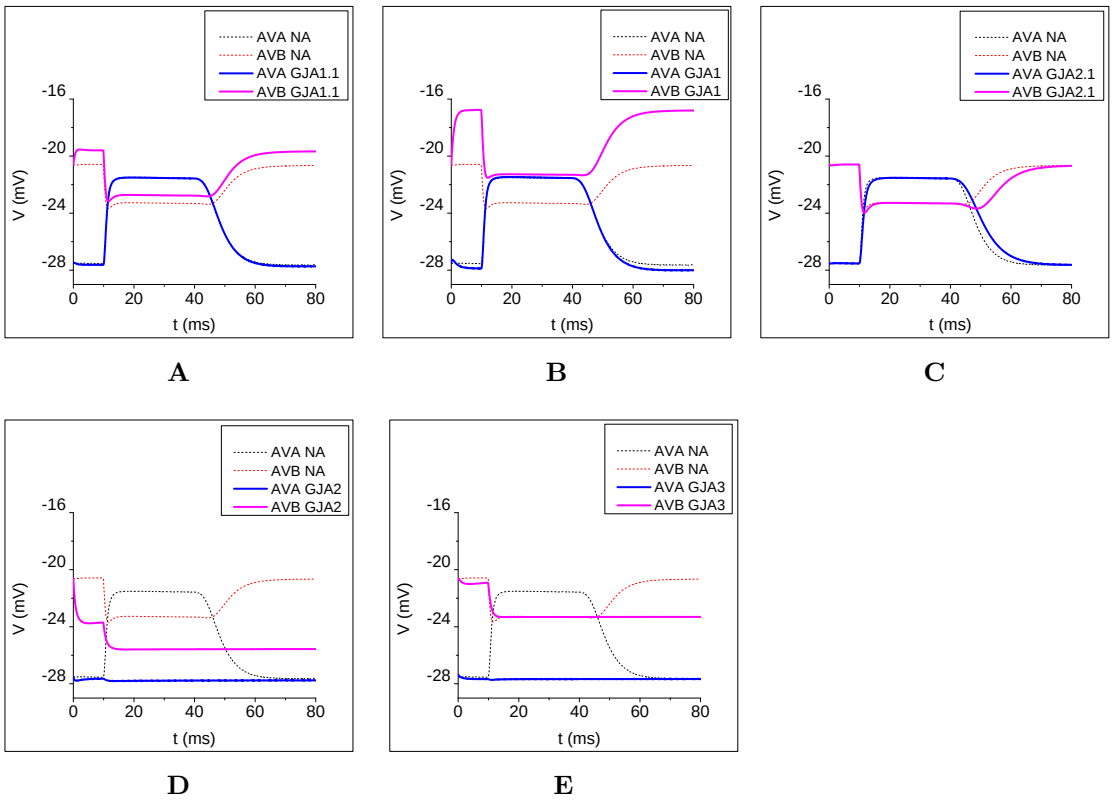

Figure 4.5: **Reducing the number of electrical synapses for most important connections of backward-responsible circuit. (A-E)** The AVA and AVB voltage levels of complete TW circuit are displayed by the black (AVA NA) and the red (AVB NA) dashed lines, respectively. **(A)** The AVB-DVA gap junctions are reduced from 2 to 1. The ablated TW circuit behaves correctly after application the anterior tap stimulus. GJA1.1 represents the TW circuit, where AVB-DVA gap junctions are reduced from 2 to 1. **(B)** Ablating both gap junctions from AVB to DVA causes the disability of TW circuit to promote backward withdrawal, because the AVB neuron misses the inhibition from DVA. GJA1.1 represents the TW circuit, where AVB-DVA gap junctions are reduced from 2 to 0. **(C)** Reducing AVM-AVD gap junction from 2 to 1 has a minimal impact on the overall output of TW circuit. GJA2.1 represents the TW circuit, where AVM-AVD gap junctions are reduced from 2 to 1. **(D)** If both of AVM-AVD gap junctions are removed, the neural network can not pass the stimulus signal from AVM sensor to interneurons. C. elegans is unable to respond with reverse locomotion. GJA2 represents the TW circuit, where AVM-AVD gap junctions are reduced from 2 to 0. **(E)** Combination of ablations from the B and D. The impacts of these two ablations are summed together. Modified TW circuit does not support reverse locomotion as a response to anterior tap stimulus. GJA3 represents combination of two synaptic ablations from B and D scenarios.

Compared to the chemical synapses, the gap junctions do not decide on the direction of locomotion, they play roles in fast signal forwarding from sensor neurons to interneurons and in correlation of membrane potentials between neurons. The pairs of the Figures 4.5A with 4.5B and 4.5C with 4.5D allows to compare the strength/weight of one gap junction. If only one of the two gap junctions is removed, the circuit still behaves correctly. Second ablation causes a total defect in correct processing of anterior tap stimulus. The different numbers of gap junctions are important to allow more complex synchronization as described in the case of AVB-DVA gap junctions. In the AVA-PVC-DVA-AVB path, the opposite signals are propagated from both end-points (AVA and AVB), the stronger one wins and sends inhibitory or excitatory signal to both of the end-points back.

4.1.3 Building the AVM stimulus processing TW circuit from scratch

In the first step, the feed-forward propagation of AVM stimulus to the layer of interneurons has to be ensured. To this end, a reduced TW circuit consisting only of 2 AVM-AVD gap junctions and 63 AVD-AVA chemical synapses (Figures 4.6A, 4.6B). Stimulating AVM sensor in such a circuit will lead to the convergence of AVA activation to the reverse potential E_{syn} of an excitatory synapse, which is 0 mV, caused by the strong excitation from AVD neuron. The AVB command interneuron does not expose any activity. In summary, this TW circuit does not recognize the stimulus episode and does not allow a default forward movement in the steady state.

In the second case – Figures 4.6C, 4.6D – we add an important inhibitory synapse from AVM to AVB, which was discussed in the Section 4.1.1, to the model from the first step. As expected, the AVB command interneuron is inhibited, which is a desired behavior. But again, the inhibition does not respond to the stimulus and converges from the beginning of the simulation to the reverse potential E_{syn} of an inhibitory synapse, which is -48 mV. Similar to the first step, the circuit does not meet the requirements for correct handling of AVM tap stimulus.

To make the AVA and AVB command interneurons mutually dependent, 27 inhibitory synapses from AVB to AVA are added Figures 4.6E, 4.6F. The excitation of AVA, caused by AVD neuron, is not balanced by the inhibition from AVB neuron, which prevents the AVA neuron to be activated at reverse potential of excitatory synapse. As a result, the AVA neuron is able to recognize the start of the tap stimulus. The membrane potential of AVB neuron stay unchanged.

In the next step, the AVB inhibition is reduced by the excitatory AVD-AVB synapse in order to prevent convergence to the reverse potential of inhibitory synapse and allow to recognize the start of the tap stimulus Figures 4.6G, 4.6H. From this point, AVB neuron weakly recognizes the start of the tap stimulus and AVA membrane potential repolarizes slightly (not visible on the graph) after the end of AVM stimulation. The impact of AVD-AVB excitatory synapse is integrated through a negative feedback connection back to the AVD neuron Figures 4.6I, 4.6J. Because of relatively low number of synapses

between AVD and AVA, the impact of this loop is hardly visible, but it is a good example how two neurons controls and synchronize each other through feedback connections.

The AVB inhibition in the steady state is still strong enough to avoid the AVM-AVB inhibitory synapses to generate visible inhibitory impact on AVB during the tap stimulus. Therefore, we add excitatory synapses from PVC to AVB to increase membrane potential of AVB in the steady state Figures 4.6K, 4.6L. The resulting TW circuit decreases the voltage difference between the AVA and AVB neurons and both of the command interneurons are able to react on the start of the tap stimulus. Note, that the default forward crawling before and after the stimulus episode is still not supported by such circuit.

Recognition of the end of the tap stimulus has not been sensed properly by the previous TW circuit. The AVD interneuron is activated when the stimulus starts, but after the end of tap, the repolarization of AVD is very slow because AVD does not receive any inhibitory input to force the activation of AVD to return back to the steady state. Despite the synaptic connections from PVC to AVD are excitatory, the PVC neuron is activated close to its steady state. Therefore, even the excitatory synapses have an inhibitory effect on high depolarized AVD neuron and force the membrane potential of AVD to fall down, after the tap stimulus is over Figures 4.6M, 4.6N. The second impact of the controlling of AVD repolarization through PVC neuron is the impact of 31 PVC-AVB excitatory synapses on AVB command interneuron Figures 4.6O, 4.6P. As long as the AVD activation decreases after the end of the tap stimulus, the PVC-AVB synapses cause an excitation to AVB, so it is able to recognize the end of the stimulus, too, and wins over the AVA membrane potential. The same situation happens before the application of tap stimulus. From this point, the TW circuit recognizes start and end of the stimulation and promote default forward locomotion, when no stimulus is applied.

The expected voltage difference between the depolarized AVA neuron and hyperpolarized AVB neuron is less than 5 mV. From the last evolution of minimal backward-responsible TW circuit we have the corresponding difference at 15 mV. By adding 10 gap junctions PVC-AVA, the membrane potential of AVA neuron synchronize with rapidly lower membrane potential of PVC and vice versa (Figures 4.6Q, 4.6R). The result of such synchronization significantly decrease the AVA voltage level and increase the PVC activation, which affects the AVB neuron. Concluding these twofold impact, the difference between AVA and AVB activations is closer to the desired value.

In the second last step, we push the AVA and AVB membrane potentials even closer by adding 28 inhibitory synapses from AVA to PVC (Figures 4.6S, 4.6T), which will amplify the synchronization described in the previous step (Figures 4.6Q, 4.6R). If the direct connection between AVD and AVB neurons are removed, the overall output will not change significantly, because of low numbers of both of the removed synapses Figures 4.6U, 4.6V. This reduced TW circuit is the final minimal backward-responsible NC.

The further incremental adding of chemical and electrical synapses does not lead to any significant changes. To shift the membrane potentials of AVB and AVA on Figure 4.6V

to the expected position, the inhibitory synapses from PVD sensor neuron to the AVA and PVC neurons are needed. PVD neuron is a polymodal sensor [58] responsible for handling cold temperatures and the intense touch event in the central body of the worm. It is functionally not related to the processing of the anterior tap. If this neuron is integrated into our TW circuit, we need to employ also the DVA interneuron with its gap junctions to the PVC and AVB neurons to balance the inhibitory signal from PVD. This behavior proves the functional dependency between the PVD and DVA neurons [2]. DVA interneuron is responsible for the modulation of both, backward and forward locomotion [2, 21]. Ablation of DVA interneuron leads to rapid decrease of forward locomotion and two-fold increase of reversals [21]. DVA is located with the DVC and DVB in dorso-rectal ganglion and does not have a left and right copy [59]. It expresses the mechanosensitive TRPN channel – TRP-4 – which is supposed to play the role of a stretch receptor [60].

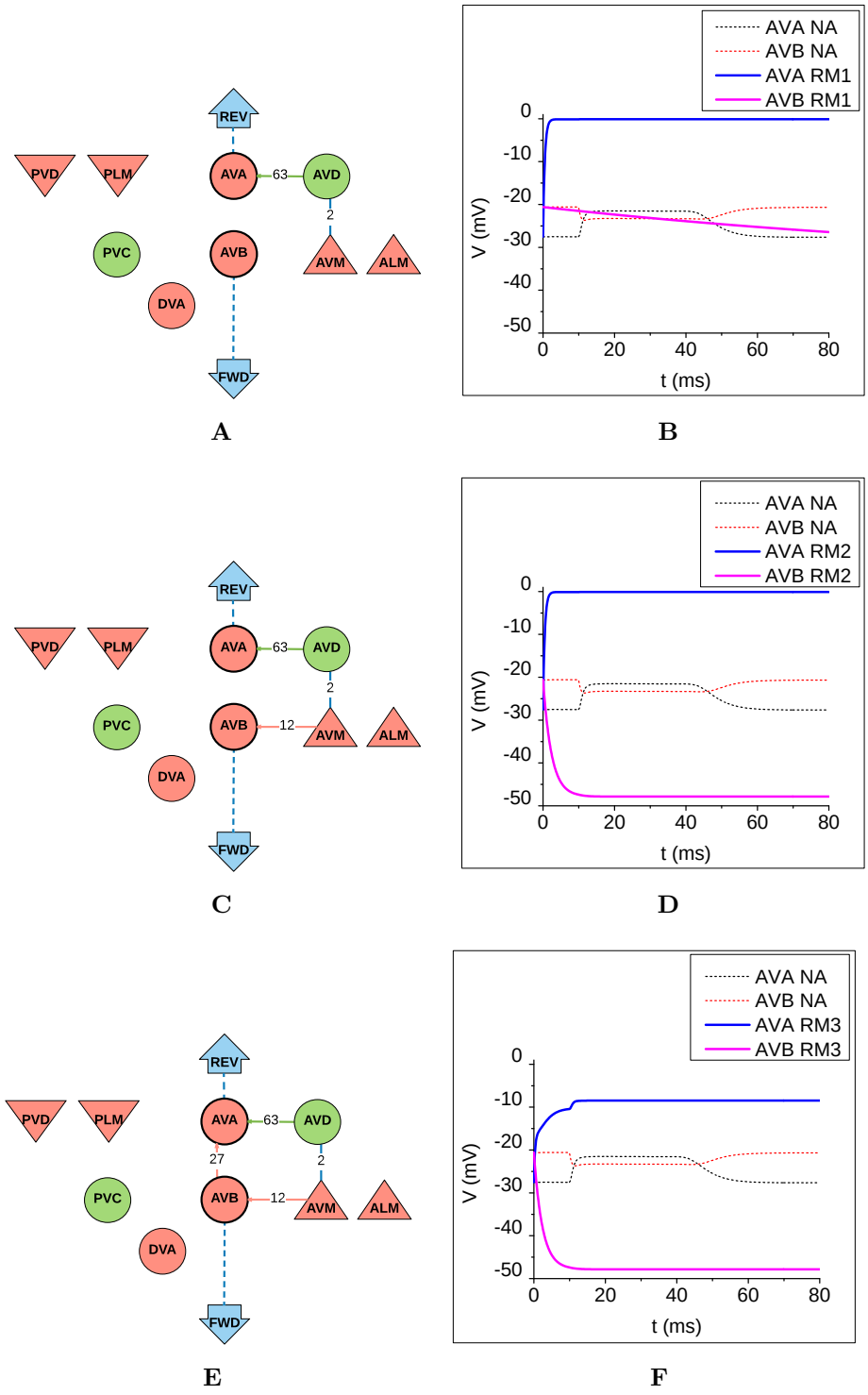

Figure 4.6: (Continued on the next page.)

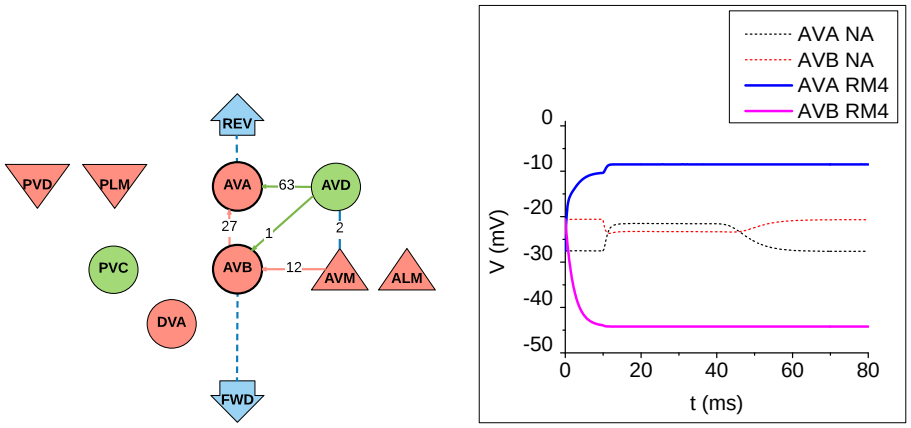

G

H

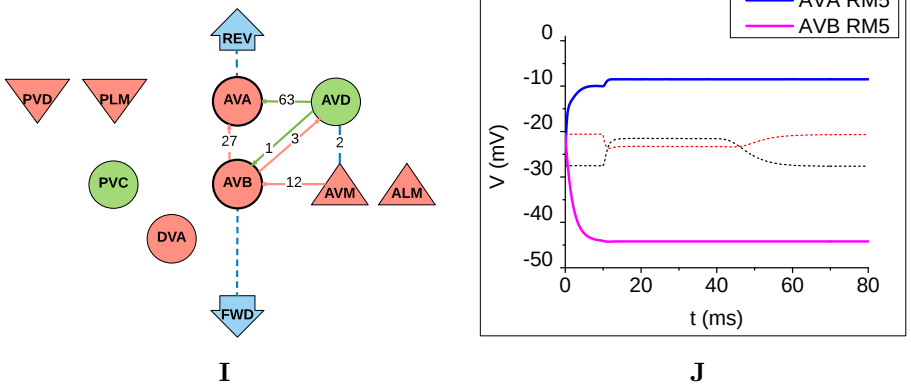

I

J

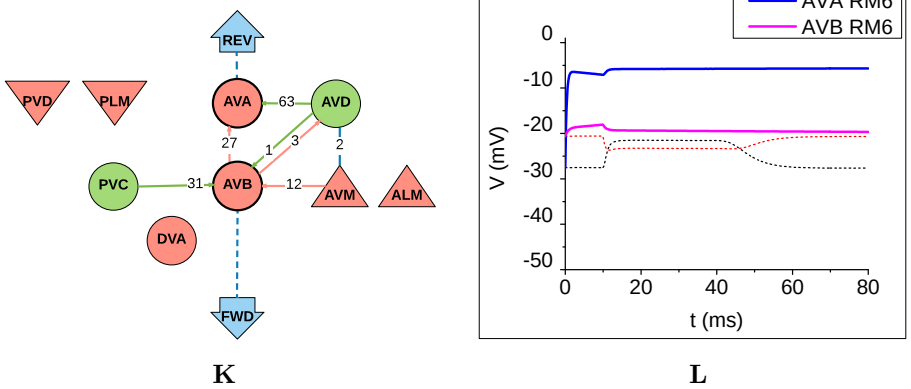

K

L

Figure 4.6: (Continued on the next page.)

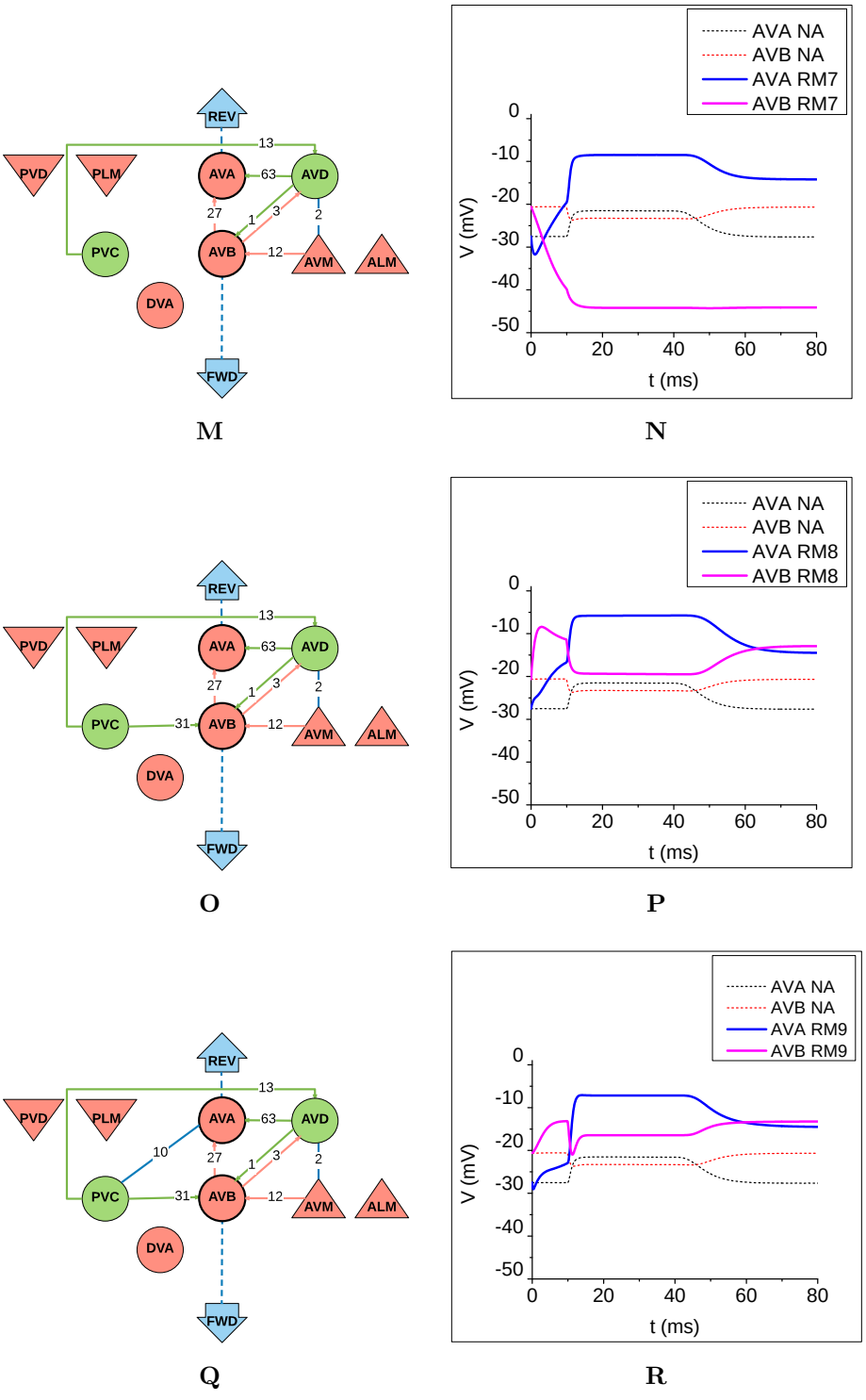

Figure 4.6: (Continued on the next page.)

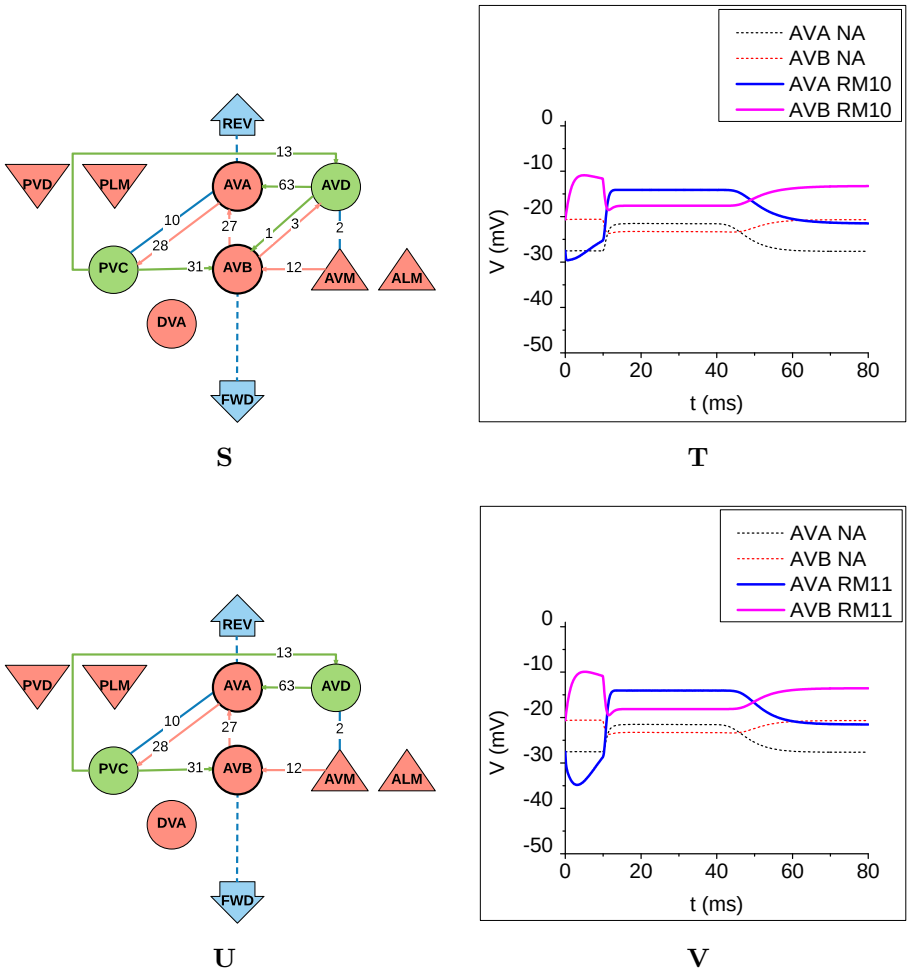

Figure 4.6: (Caption on the next page.)

Figure 4.6: **Building the minimal backward responsible TW circuit by adding synapses stepwise from scratch. First column** Wiring models of the stepwise built TW circuits. **Second column** The AVA and AVB voltage levels of the complete TW circuit are displayed by the black (AVA NA) and the red (AVB NA) dashed lines, respectively. **(A-B)** Most simple TW circuit passing the tap stimulus from AVM sensor to the AVA command neuron. AVA and AVB neurons are not able to recognize tap stimulus. AVA rises up right after the start of simulation to the reverse potential of excitatory synapse. **(C-D)** Added inhibitory chemical connection AVM-AVB to the model from A. The inhibition of AVB is initiated after the start of the simulation and converges to the reverse potential of inhibitory synapse. AVA and AVB neurons are not able to recognize tap stimulus. **(E-F)** Adding inhibitory synapse AVB-AVA has an inhibitory effect on AVA during steady state and prevent to converge to 0 mV. From this point AVA is able to recognize the start of the tap stimulus. **(G-H)** In order to prevent massive inhibition of AVB, excitatory synapse AVD-AVB is added. The AVB is from now able to recognize the tap stimulus event and AVA weakly (not visible on the graph) recognizes also the end of stimulus. **(I-J)** Negative feedback through AVB-AVD inhibitory synapse amplify the controlling of AVD neuron through AVB. **(K-L)** The AVB inhibition is prevented by excitatory synapses from PVC. They have no impact on processing of the tap stimulus, because there is no incoming synapse to PVC, but they modify the steady state of AVB in order to stronger recognize the start of the tap stimulus. **(M-N and O-P)** Added 13 excitatory synapses PVC-AVD to modulate the falling phase of AVD membrane potential after the tap stimulus is done. PVC neuron receives no activation during simulation, so even the excitatory synapses from PVC to AVD have an inhibitory effect on high depolarized AVD, which results into stronger recognizing the end of tap stimulus by AVA and AVB, too. The M-N display the impact of PVC-AVD synapses without PVC-AVB connection. It is visible, that PVC-AVD synapses modulate the AVA repolarization and together with PVC-AVB synapses, they depolarize the AVB neuron. **(Q-R)** PVC-AVA gap junctions are added to decrease the difference in voltage potentials between AVB and AVA command neurons. The AVB activation is able to outperform AVA membrane potential after the tap stimulus is over. **(S-T)** 28 AVA-PVC inhibitory synapses is used to decrease the AVA depolarization through inhibition of PVC and sharing this inhibitory effect with AVA through strong electrical coupling. **(U-V)** Direct synaptic connections between AVD and AVB neurons have a very small impact on the correct processing of anterior tap stimulus. They can be removed without visible impact on the TW circuit. The resulted TW circuit can be considered as the minimal backward responsible controller.

4.1.4 Neurons ablations

In the experiments, all of the neurons were ablated one after another except the command interneurons – AVB and AVA – and the sensory neuron – AVM – which is responsible for sensing the anterior tap event (Figure 4.7D). The reason is to compare the voltage potentials of their membranes as they are directly supposed to control the motor neurons for the forward and backward locomotion. Comparing the results of the ablations (Figure 4.7D) it is observed, that ablation of AVD, PVC and DVA interneurons have the biggest influence to the TW circuit output. Ablation of AVD neuron (Figure 4.7A) implies inability of AVA neuron to depolarize during the anterior tap and by that, initiate the backward locomotion. Also the AVB is unable to react on the end of the stimulation, because AVD interneuron is suppose to sense the end of the stimulus pulse. On the

other hand, the knocking out of the PVC interneuron (Figure 4.7B) causes the circuit generate backward locomotion during the entire simulation run, because the AVB neuron, responsible for forward locomotion, receives no activation before and after the application of stimulus. Specific scenario arises by ablation of the DVA interneuron. This neuron is supposed to have an inhibitory impact on AVB neuron. If DVA is missing, both command neurons are able correctly recognize the start and end of the stimulus, but because of missing inhibition from DVA, AVB membrane potential outperforms the AVA depolarization and prevents C. elegans to move backward as a response to the anterior tap (Figure 4.7C). Ablation of the other neurons does not have a significant impact on the TW circuit output, signaling, the AVD interneuron is the crucial control unit for correct processing of the AVM stimulus. It receives the stimulus signal from the AVM sensor and initiates the activation of backward-responsible AVA command interneuron.

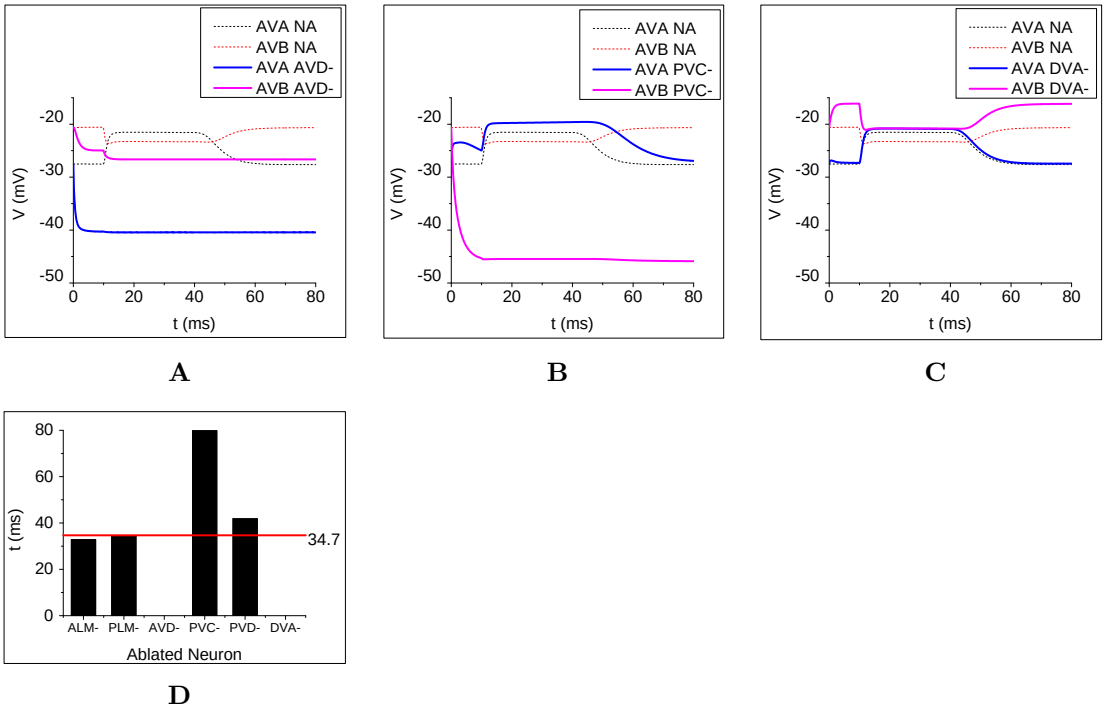

Figure 4.7: **Impact of neuronal ablations in TW circuit on processing of the anterior tap stimulus. (A-C)** Comparison of AVA and AVB voltage traces of complete TW circuit with the circuits lacking one neuron. AVA and AVB membrane potentials are displayed with the black and red dashed lines, respectively. The anterior tap is applied to the AVM sensor neuron. **(A)** Voltage traces of TW circuit missing the AVD interneuron. Since the AVD interneuron controls the activation of AVA neuron during the anterior tap, its absence leads to inactivation of AVA. The nematode is unable to move backwards as a response to the anterior tap. **(B)** Voltage traces of TW circuit missing the PVC interneuron. The AVB command interneuron receives only weak excitation from AVD. Therefore, the AVB membrane potential hyperpolarizes close to reverse potential of inhibitory synapse. The AVA voltage level is higher then AVB during the entire simulation. **(C)** Voltage traces of TW circuit missing the DVA interneuron. DVA interneuron has an inhibitory impact on AVB and if it is missing, the membrane potential of AVB is shifted to the higher values and AVA activation is unable to outperform it during the tap stimulus. **(D)** Comparison of impacts of single neurons ablations to the period spent by worm on reverse locomotion. Ablation of AVD or DVA neurons lead to complete lost of revere movement. On the other hand, the ablation of PVC disable the AVB neuron and the worm is moving backwards also before and after the stimulation. The red horizontal line shows the time spent on reverse movement of C. elegans when no neuron is ablated.

4.2 Posterior tap reflex

We assume a posterior tap as a pulse stimulus to the PLM sensor neuron. There is also second posterior sensor neuron called PVD, but it is supposed to be a polymodal nociceptor responsible for sensing the harsh-touch in the central region of the worm and

the cold temperatures [13]. Animals lacking this neuron are still able to respond to the anterior and posterior tap.

4.2.1 Forward time period analysis

Following table 4.3 lists the crucial chemical synapses for correct promoting of forward withdrawal to the posterior tap. As a matter of fact, there are only PVC-AVB synapses having visible impact on the time spent on the forward locomotion (Figure 4.8A). Ablating at least 16 synapses out of 31 leads to a rapid decrease or complete lost of ability to move forward as a reaction to the PLM tap stimulus. PVC express excitatory synapses to its postsynaptic targets and missing the connections between PVC and AVB neurons, the depolarization of the AVB neuron is significantly lower at average -6.75 mV and by that outperformed by the AVA activation Figure 4.8B. It implies, that the minimal requirement on the number of PVC-AVB connections are 16 synapses Figure 4.8A.

Ablation of other chemical synapses (always only between one couple of neurons) have none or very little impact on the time spent by the worm on crawling forward. They modulate the forward behavior but from the time analysis point of view, their ablation do not lead to a significant change in time, as the AVB activation is higher then AVA activation by default. So even the reduced TW circuit does not recognize the stimulus, the AVB membrne potential is still over AVA membrane potential and C. elegans moves forward. The deeper analysis will be provided in the voltage traces analysis (Section 4.2.2).

Table 4.3: Most important chemical synapses for processing of the posterior tap. The F_{NA} represents the time spent on forward locomotion when no ablation is performed, δ_{FWD} specifies time change percentage.

F_{NA} = 801 ms			
Electrical synapse			
From	**To**	**N**	**δ_{FWD}**
PVC	AVB	from 0/31 to 15/31	-37.45 – -98.75.4%

The analysis of the neuronal electrical couplings exhibits following results (Table 4.4). The electrical coupling between neurons AVA and PVC consists of 10 gap junctions and ensures synchronization between the connected neurons Figure 4.8B. If all of these electrical synapses are missing, we can observe a decrease more than 50.81% of the time spent on the forward locomotion (Figure 4.11B). This is caused as a result of higher activation of AVA before and after the stimulation. The response of TW circuit during the stimulation is still forward withdrawal. Ablating only 9 out of 10 gap junctions will not cause the disability to crawl forward before and after the stimulus episode

(Figure 4.11A). If the AVA-PVC gap junctions are not missing, the activated AVA neuron synchronizes the PVC neuron which in turn sends a stronger activation to the AVB. Finally, AVB inhibits the AVA neuron, which results in decrease of membrane potential of AVA. Concluding this procedure, AVA-PVC electrical coupling supports the inhibition of AVA neuron through the AVB. It is also part of the AVA-PVC-DVA-AVB gap junctions pathway providing an intrinsic bias toward a forward locomotion as a default behavior when no stimulus is applied.

Table 4.4: Most important electrical synapses for processing of the posterior tap.

$\mathbf{F_{NA} = 801\ ms}$			
Electrical synapse			
From	**To**	**N**	$\delta_{\mathbf{FWD}}$
PVC	AVA	0/10	-50.81%

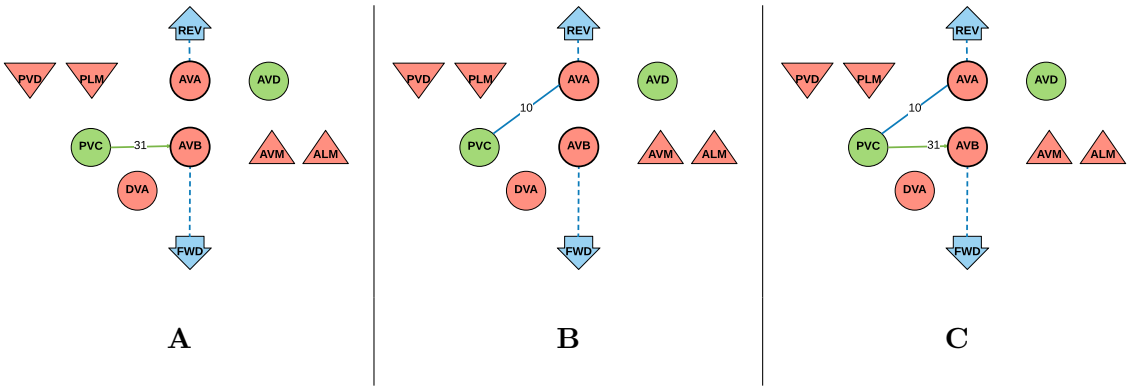

Figure 4.8: **Most important chemical and electrical synapses in TW circuit for forward locomotion. (A)** The most important chemical synapses AVA-PVC gain activation for forward-responsible AVB neuron. **(B)** The most important gap junctions responsible for correlation of membrane activations of AVB and AVA neurons.**(C)** Simplified TW circuit consisting of chemical synapses from (A) and gap junctions from (B) represents the necessary skeleton for processing of posterior tap stimulus.

The most important results of the time analysis of handling the posterior tap are (i) the correlation of neurons connected by the gap junctions combined with the chemical synapses and (ii) the role of gap junctions in providing an intrinsic bias toward forward locomotion. The roles of the chemical synapses in the posterior tap processing are straightforward.

4.2.2 Voltage traces analysis

The time analysis data (Section 4.2.1) are extended in this section by investigations on the impact of synaptic ablations of the AVA and AVB command interneurons.

First, the voltage traces of AVA and AVB neurons in the complete TW circuit (NA) are shown in the Figure 4.9. The positive change of voltage of AVA and AVB neurons after applying the posterior tap stimulus to the PLM neuron is almost equal – both command interneurons are activated, which corresponds to concurrent activations of the backward and forward sub-circuits after applying the tap stimulus [9, 10]. The difference between the AVB and AVA activations is in average 6.76 mV.

Figures 4.10A, 4.10B display the minimal requirement 16 synapses on PVC-AVB chemical synapse in order to support forward locomotion as a response to the posterior tap stimulus (Figure 4.10A). Since the underlying synapse is supposed to be excitatory, reducing the number of synapses to 15 causes a lower activation of AVB neuron at -6.75 mV, which results into outperforming of AVB activation by the AVA membrane potential during the stimulus event (Figure 4.10B). During performed ablations, voltage traces of AVA command interneuron remains unchanged, indicating that ablated PVC-AVB synapses does not impact the backward-responsible sub-circuit.

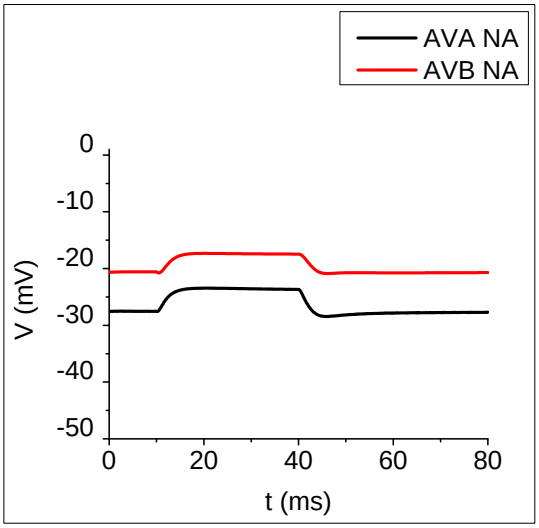

Figure 4.9: **Membrane potentials of the AVB (red) and AVA (black) neurons during posterior tap stimulus.**

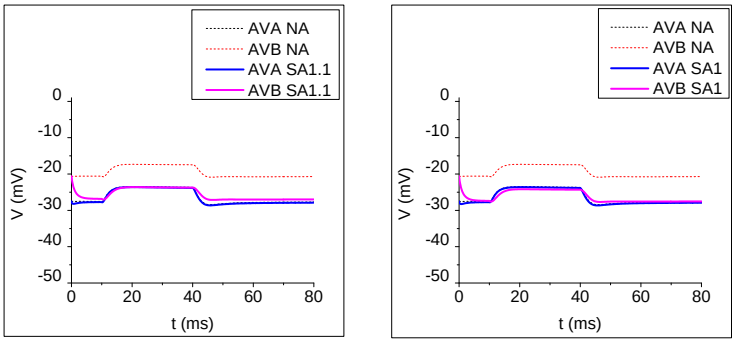

A **B**

Figure 4.10: **Reducing the number of chemical synapses for most important connections of forward-responsible circuit. (A-B)** The AVA and AVB voltage levels of the TW neural circuit without any ablation are displayed by the black (AVA NA) and the red (AVB NA) dashed lines, respectively. **(A)** The minimum multiplicity of the PVC-AVB synapse, when the worm still responds with the forward movement to the posterior tap stimulus applied to the PLM sensor neuron. Because the PVC-AVB synapse is supposed to be excitatory, excitation of the AVB interneuron is lower at 6.76 mV. SA1.1 represents TW circuit with PVC-AVB synapses reduced from 31 to 16. **(B)** Reducing the number of PVC-AVB synapses to 15 implies the inability of forward withdrawal as a response to the posterior tap. The activation of backward-responsible neuron AVA is higher than membrane potential of AVB. SA1 represents TW circuit with PVC-AVB synapses reduced from 31 to 16.

Time analysis of the TW circuit in respect to promoting forward withdrawal (Section 4.2.1) identified only PVC-AVB gap junctions as a critical point for correct processing of posterior tap. If all 10 gap junctions are ablated, the AVA membrane potential increases in average at 5 mV, and outperforms the AVB steady state (before and after the stimulus) membrane potential (Figure 4.11B). If only 9 out of 10 gap junctions are ablated, the incorrect behavior, before and after the stimulation, is suppressed (Figure 4.11A).

The time analysis does not revealed any change in the time spent on forward locomotion when PLM-PVC gap junction is ablated. Voltage analysis, on the other hand, identified a significant disruption in AVA and AVB membrane potentials. Because of inhibitory nature of PLM neuron, tap stimulus current could not be passed to interneurons, which results into inability of PVC interneuron to activate AVB command neuron (Figure 4.11C). In the next step, we investigated the impact of other two possibly related gap junctions PVC-DVA and DVA-AVB. From the time analysis of backward-responsible TW circuit (Section 4.1.1), we already know, that the two DVA-AVB gap junctions have an inhibitory effect on membrane potential of AVB. We examined the role of DVA-AVB gap junctions on the complete TW circuit missing the 10 PVC-AVA gap junctions (Figure 4.11D).Ablation of all PVC-AVA gap junctions lead to incorrect behavior before and after the tap stimulus. Further ablation of DVA-AVB gap junctions fixes this undesired

behavior by removing the inhibitory impact of DVA on AVB neuron. Similar inhibitory impact on AVB activation can be observed on the PVC-DVA gap junction. The negatively charged DVA interneuron weakens the depolarization of the PVC interneuron, through the gap junction which impacts also the depolarization of the AVB neuron. Removal of PVC-DVA gap junction also balances the negative impact of PVC-AVA gap junctions removal (Figure 4.11E). The last experiment combines together ablations of PVC-AVA, PVC-DVA and DVA-AVB (Figure 4.11F). As expected, the impacts of ablations of PVC-DVA and DVA-AVB are summed together and balance the negative impact of PVC-AVA ablations.

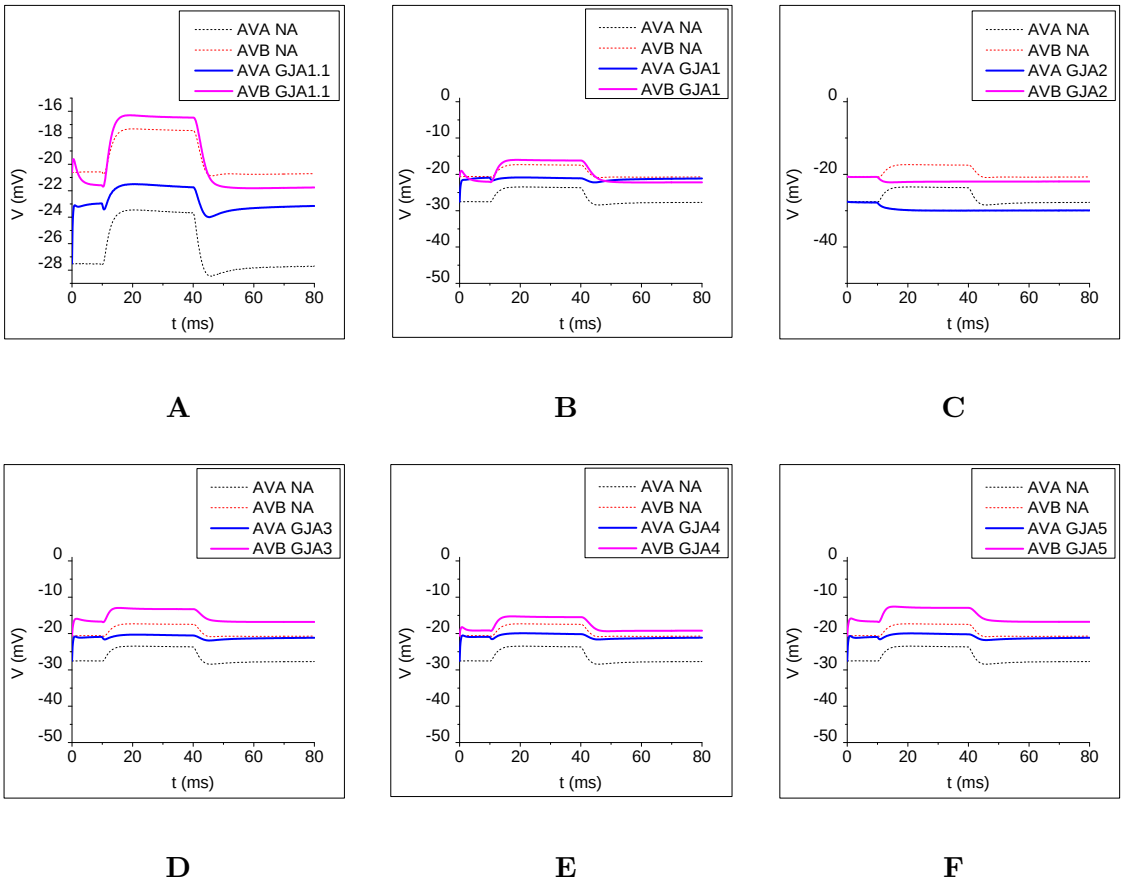

Figure 4.11: (Caption on the next page.)

Figure 4.11: (Previous page.)**Reducing the number of electrical synapses for most important connections of forward-responsible circuit. (A-F)** The AVA and AVB voltage levels of the locomotory neuronal circuit without any ablation are displayed by the black (AVA NA) and the red (AVB NA) dashed lines, respectively. **(A)** At least one gap junction from PVC to AVA is required to keep the correct output of TW circuit to posterior tap stimulus. GJA1.1 represents the TW circuit missing 10 out of 10 PVC-AVA gap junctions. **(B)** Ablation of all PVC-AVA gap junctions leads to the lost of default forward crawling before and after the tap stimulus. GJA1 represents the TW circuit missing 10 out of 10 PVC-AVA gap junctions. **(C)** PLM-PVC gap junction enables to pass the stimulus pulse into interneurons. Missing this connection, TW circuit recognizes (negatively) only the start of stimulation. GJA2 represents the TW circuit missing 1 out of 1 PLM-PVC gap junction. **(D)** Combination of ablations from the B and ablation of the 2 DVA-AVB gap junctions. Missing DVA-AVB electrical synapses balance the negative impact of ablated PVC-DVA gap junctions on AVB voltage potential. GJA3 represents the TW circuit missing 2 out of 2 DVA-AVB gap junctions and 10 out of 10 PVC-AVA gap junctions. **(E)** Combination of ablations from the B and ablation of the 1 PVC-DVA gap junction. Missing PVC-DVA electrical synapse weaken the negative impact of ablated PVC-DVA gap junctions on AVB activation. GJA4 represents the TW circuit missing 1 out of 1 PVC-DVA gap junctions and 10 out of 10 PVC-AVA gap junctions. **(F)** Combined ablations from the B, D and E scenarios. Ablation of PVC-AVA gap junctions is balanced by the summed impact of DVA-AVB and PVC-DVA ablations. GJA5 represents the TW circuit missing 1 out of 1 PVC-DVA gap junctions, 2 out of 2 DVA-AVB gap junctions and 10 out of 10 PVC-AVA gap junctions.

4.2.3 Building the PLM stimulus processing TW circuit from scratch

Based on the information from Section 3.2 we start with the model of TW circuit with no chemical or electrical synapse (Figures 4.12A, 4.12B) to find an evidence of default propagation of the forward locomotion. In such a circuit the membrane potential of AVB is higher than AVA activation during the entire simulation time. In our case it is achieved by the higher resting potential of AVB neuron compared to the AVA neuron. The potential curves linearly decrease during the simulation, since the neurons does not receive any synaptic, electric or external current and the membrane of neuron leaks specific current dependent on its physiological properties. In the next step, we employ very simple pathway to propagate the input current through the PVC interneuron to the AVB command neuron (Figures 4.12B, 4.12C). Due to the excitatory synapses PVC-AVB, the AVB activation converges to the reverse potential of the excitatory synapse, which is equal to 0 mV. The AVA neuron does not get stimulated. it remain unchanged to the previous experiment. Then, we model the sensitivity of the AVB command neuron on the start and end of posterior tap stimulus. The excitation of AVB from PVC neuron needs to be balanced by inhibitory impact ensured by gap junctions pathway PVC-DVA-AVB on one hand (Figures 4.12E, 4.12F), and AVA-AVB together with AVA-PVC and AVM-AVB inhibitory synapses on the other hand (Figures 4.12H, 4.12J, 4.12J). In both cases, negatively charged inhibitory neuron (DVA, AVA) balances the PVC excitatory role. Note that AVM-AVB chemical synapses are more related to the backward-responsible subcircuit (Section 4.1.3), but they are also essential in order to modulate AVB membrane

potential in the steady state.

The final three experiments (Figures 4.12N, 4.12P, 4.12R) are supposed to co-activate the AVA command interneuron to the expected values. The depolarization of AVA is ensured by the strong electrical coupling AVA-PVC (Figures 4.12M, 4.12N), which synchronizes the PVC depolarization with the AVA neuron. Since the depolarization of AVA is quite higher than the expected values, it needs to be decreased by adding the AVB-AVA inhibitory synapses (Figures 4.12O, 4.12P). The membrane potential of AVA in the steady state is modulated by the excitatory synapses PVC-AVA, balancing the impact of inhibitory synapses targeting AVA neuron (Figures 4.12Q, 4.12R). We assume the model on Figure 4.12E a minimal forward-responsible TW circuit answering with the forward withdrawal to the posterior tap.

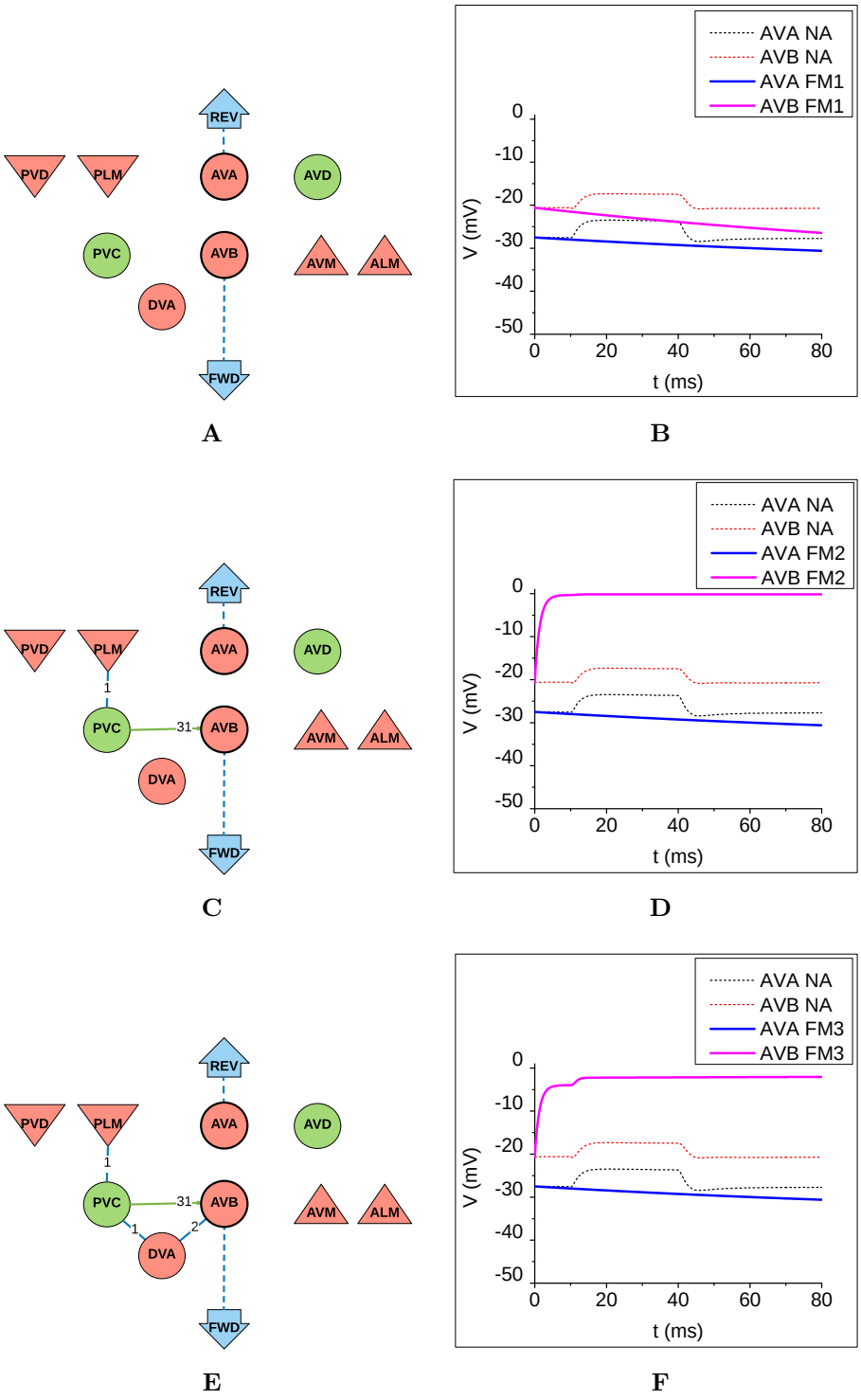

Figure 4.12: (Continued on the next page.)

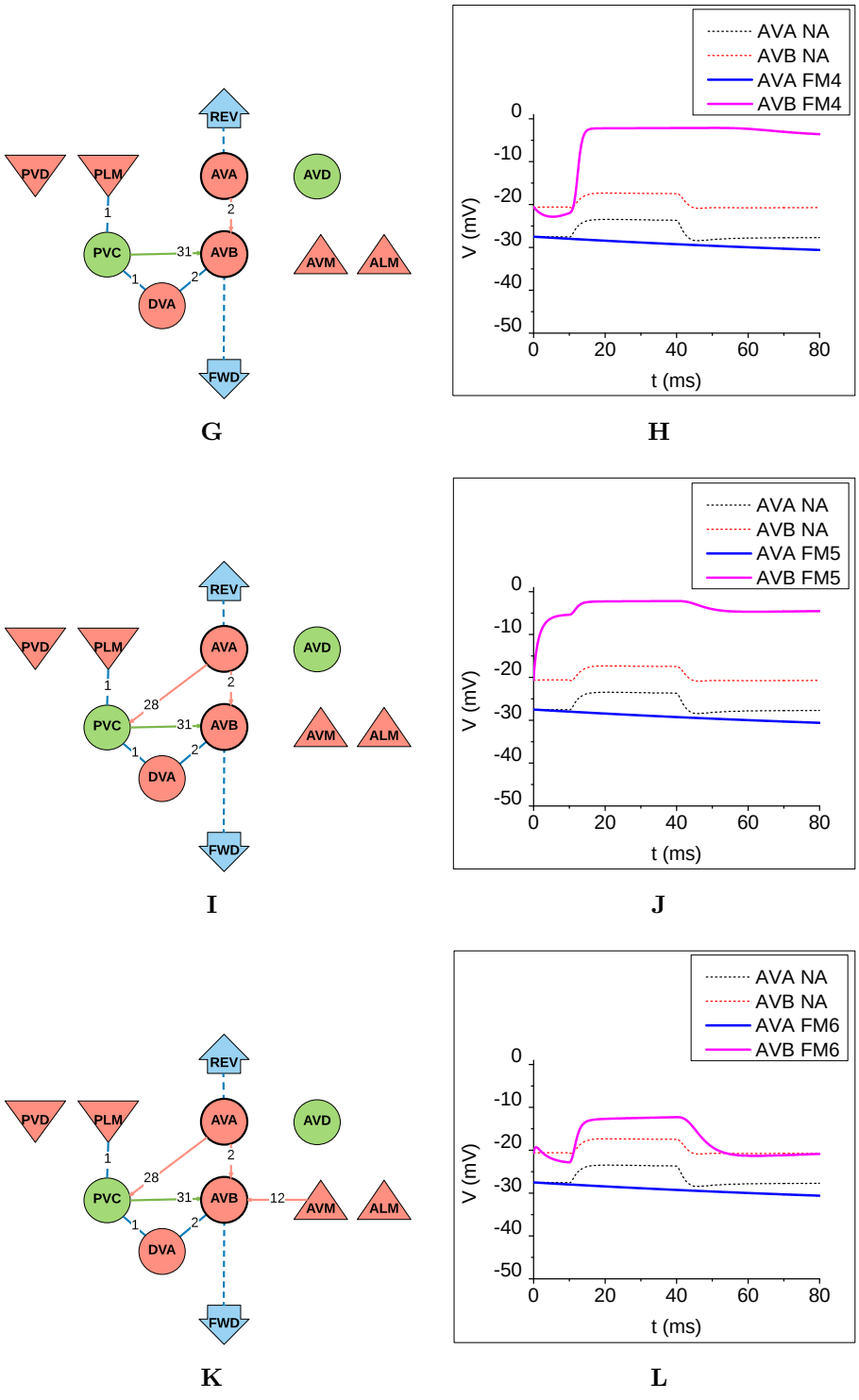

Figure 4.12: (Continued on the next page.)

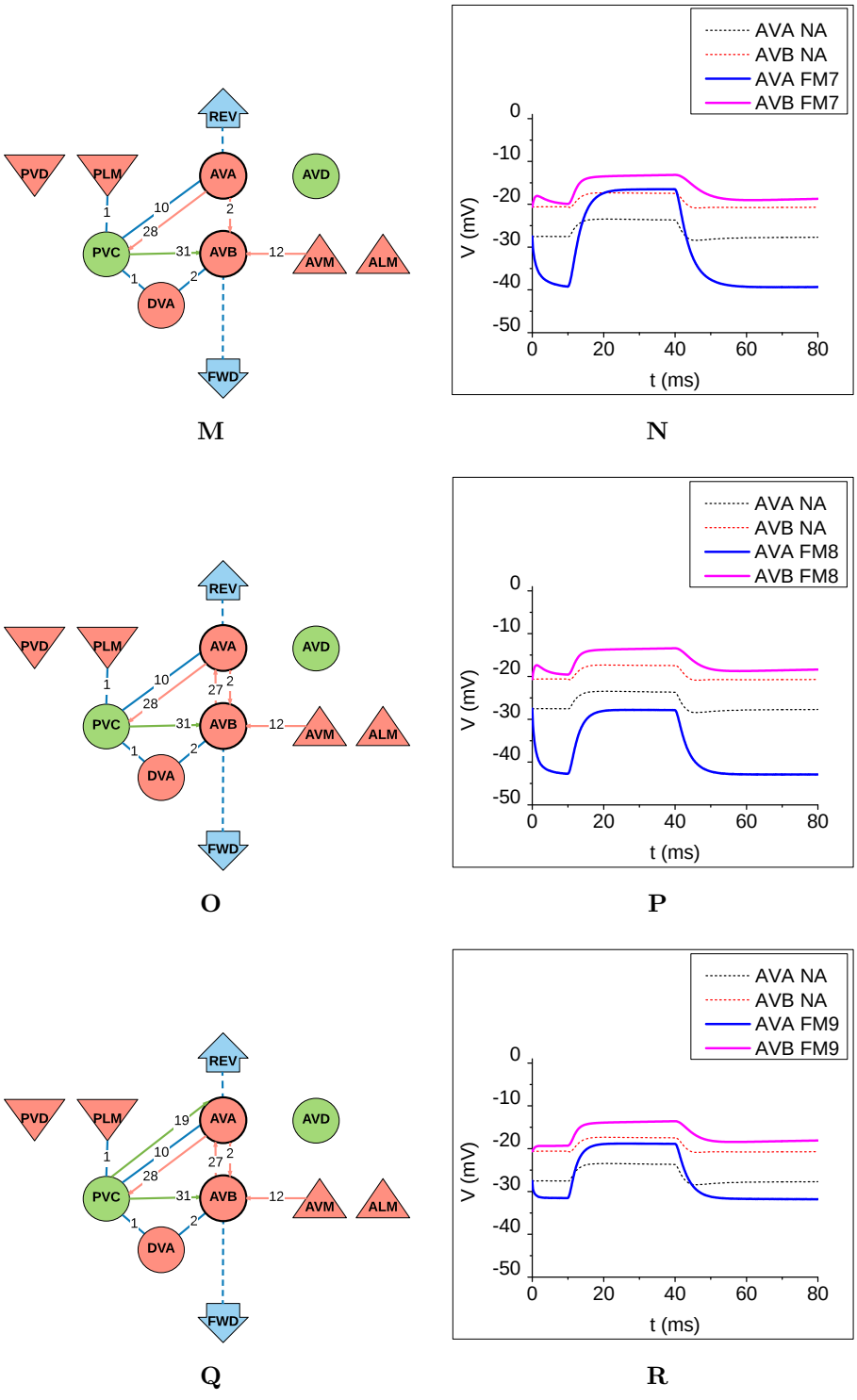

Figure 4.12: (Caption on the next page.)

Figure 4.12: **Building the minimal forward-responsible TW circuit stepwise from scratch. First column** Wiring models of the stepwise constructed TW circuits. **Second column** The AVA and AVB voltage levels of the complete TW circuit are displayed by the black (AVA NA) and the red (AVB NA) dashed lines, respectively. **(A-B)** TW circuit without any chemical or electrical synapse. Because of higher AVB resting potential, the activation of AVB is stronger then activation of AVA and therefore theoretically the worm moves forward during the entire simulation time. This scenario captures part of the mechanisms supporting forward locomotion by default. **(C-D)** The minimal connections for passing the stimulus current to the AVB command interneuron. AVA activation remains unchanged, AVB depolarizes to the resting potential of excitatory synapse, because of excitation from PVC neuron. The circuit is not able to recognize posterior tap stimulus. **(E-F)** The gap junctions pathway PVC-DVA-AVB is added in order to provide inhibitory input to the AVB neuron. From this point, AVB command interneuron is able to recognize the start of the stimulus. AVA is unchanged. **(G-H)** To amplify the inhibitory effect of gap junctions PVC-DVA-AVB, we add AVA-AVB inhibitory synapse. AVB neuron slightly recognizes the end of the stimulus, while the AVA command neuron is still without any activity. **(I-J)** PVC depolarization is forced to repolarize after the end of the tap stimulus by the AVA-PVC inhibitory synapse. This step will emphasize the inhibitory effect of AVA-AVB chemical synapses and PVC-DVA-AVB gap junctions when the stimulus is over. **(K-L)** AVB activation curve is shifted down closer to the expected values by adding the AVM-AVB inhibitory synapses. This inhibition also amplifies the depolarization of AVB neuron during the posterior tap stimulus. **(M-N)** To achieve the expected co-activation of AVA neuron, we add the AVA-PVC gap junctions, which causes slight inhibition to PVC and therefore also to AVB, but much higher excitation of AVA. The membrane potentials of PVC and AVA are correlated. AVA command interneuron recognizes the start and end of the stimulus. **(O-P)** Adding the inhibitory synapses from AVB to AVA will decrease the activation of AVA during the tap stimulus. This synapses support the mutually inhibition of AVB and AVA neurons. **(Q-R)** In the final step, we increase the steady state membrane potential of AVA by adding the excitatory synapses from PVC to AVA. The voltage traces of AVA and AVB are closed to the traces of the complete TW circuit. We can assume this reduced TW circuit as an minimal forward-responsible NC.

4.2.4 Neurons ablations

By performing the single neuron ablations, we investigate the impact of missing sensor neurons and interneurons to the overall output of the TW circuit. From the Figure 4.13D the most ablations have no impact on the time spent on the forward movement when posterior stimulus is applied. Also ablated neurons, involved in the building of the minimal forward-responsible TW circuit (Figures 4.12A – 4.12R) like DVA, does not change the behavior of C. elegans during the posterior tap. Most of the neurons have modulatory role on AVB and AVA membrane potentials in respect to the forward locomotion, so no visible change in respect to the time spent on forward crawling is observed. The most influencing neuronal ablation is the PVC ablation (4.13A). This neuron is supposed to be the major driver of the AVB activation during the posterior tap event. In this case, the AVA command interneuron receives sufficient activation from AVD neuron to win over the inhibited AVB neuron, which implies an incorrect response of C. elegans to the posterior tap. It is also obvious, that neither AVA nor AVB is able to recognize the start and the end of the stimulation. Ablation of AVD interneuron

(4.13B) does not bring any change to the output of the TW circuit compared to the observations regarding the processing of anterior tap (Section 4.1.4). The AVA receives much less activation because of missing excitatory synapses from AVD neuron. This effect has no significant impact on the activation of AVB command interneuron, therefore the nematode behaves correctly under such an ablation.

An interesting behavior is observed by the ablation of ALM sensor neuron(4.13C). This is a first evidence of a strong influence of sensor neuron, responsible for sensing tap stimulus in different part of the worm's body, to the output of the TW circuit. ALM has only few inhibitory chemical synapses to the interneurons (AVD and PVC) and two gap junctions to the AVM. Knocking the ALM sensor out will revert the depolarization of AVB during tap stimulus to inhibition. When the PLM stimulus is applied, the PVC interneuron receive the pulse stimulus and transmits it through 13 excitatory synapses to the AVD interneuron. In the AVD, the excitation is balanced by the inhibitory impact of the gap junctions from AVM connected with ALM and ALM-AVD inhibitory synapse. When the ALM sensor neuron is missing, this negative compensation is lower, which allows the AVA neuron to receive a higher activation from AVD than AVB from PVC (Figure 4.13C). The AVD depolarization is synchronized by the gap junctions with the AVM sensor neuron, inhibiting the AVB neuron through its 12 inhibitory synapses. This is the reason why the AVB neuron is inhibited during the posterior tap when ALM neuron is missing.

This experiment demonstrates the neurons which play the crucial role in controlling the correct signal propagation from PLM sensor neuron through the layer of interneurons to the forward-responsible motor neurons. The presence of the PVC neuron as the controlling unit which ensures the excitation of the AVB, is mandatory to enable the forward locomotion. Furthermore, ALM neuron is important to keep the AVA activation lower than AVB, otherwise it will disable the AVB neuron during the posterior tap period.

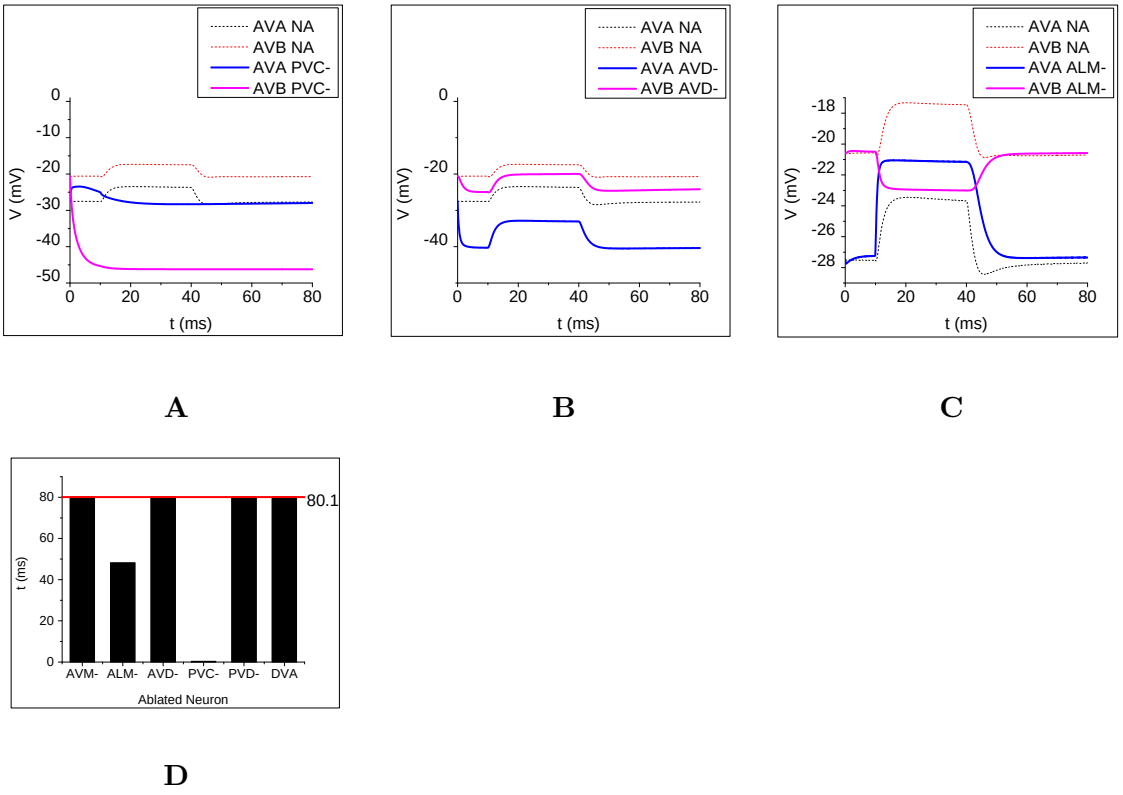

Figure 4.13: **Impact of neuronal ablations on processing of the PLM tap stimulus by TW circuit. (A-C)** Comparison of voltage traces for complete TW circuit with the circuits lacking one neuron. AVA and AVB membrane potentials are displayed with the black and red dashed lines, respectively. The posterior tap is applied to the PLM sensor neuron. **(A)** The voltage traces of TW circuit missing the PVC interneuron. Because of non-presence of PVC, AVB and AVA command interneurons do not receive any excitation, generated by the PLM sensor neuron. The AVA inhibition is compensated by the excitation from AVD neuron preventing AVA membrane potential to inhibit to the reverse potential of inhibitory synapse, similar to the AVB. **(B)** The voltage traces of TW circuit missing the AVD interneuron. TW circuit responds correctly to the posterior tap, the membrane potential of AVA is shifted to lower values because of missing excitation from AVD neuron. **(C)** Ablation of ALM sensor neuron leads to inhibition of AVB. Because of missing ALM sensor neuron, the AVD activation is higher which results into a higher AVA and ALM activation, which in turn deactivates the AVB neuron. **(D)** Comparison of impacts of single neuronal ablations to the time spent by worm on forward movement. Ablation of PVC leads to complete lost of ability to move forward. Also ablation of ALM impacts markable the forward time. The red horizontal line is equal to the time of moving forward when no neuron is ablated.

4.3 Merging of forward- and backward-responsible minimal circuits together

In this section, the minimal backward- and forward-responsible TW circuits are merged together to study possible interactions between them.

If the minimal anterior and posterior tap processing circuits (Sections 4.1.3 and 4.2.3) are put together, following circuit is obtained Figure 4.14A. Some of the electrical (AVA-PVC) and chemical (PVC-AVB, AVA-PVC and AVB-AVA) synapses are present in both minimal circuits. Therefore, these are assumed to support both, forward and backward withdrawal. On the other hand, the connections specified for only one minimal circuit may impact the correct behavior of the opposite minimal circuit. To this end, tap stimulus is applied first to the AVM sensor and second, to the PLM sensor neuron. The anterior tap (Figure 4.14B) is processed correctly with only small shift of membrane potentials of AVA and AVB to the values of complete TW circuit. On the Figure 4.14C, the PLM tap stimulus is applied expecting the forward withdrawal. In the result, the AVB depolarization is during all simulation time higher than depolarization of AVA neuron – C. elegans is moving forward. Compared to the minimal circuit for forward movement (Figure 4.12R), the AVA depolarization is much closer to the AVB voltage level because of excitatory pathway PVC-AVD-AVA. Despite the response to the posterior tap is correct, we can decrease the AVA activation by adding the inhibitory synapses PLM-AVD and PLM-AVA. These synapses were omitted in forward-responsible minimal circuit, because this circuit does not contain the AVD-AVA excitatory synapses. Summarizing the results of merged circuit we are able to formulate following hypothesis: If two circuits, each supporting the processing of one stimulus, are merged together, the resulting merged circuit is able to correctly process both of the stimuli.

Analysis of the differences in the presence of synapses between the complete TW circuit and the merged circuit suggests, that there are many synapses not necessarily required for the correct processing of anterior/posterior tap stimulus. In particular, following numbers of electrical and chemical synapses are required in the merged circuit on Figure 4.14A compared to the complete TW circuit (the not used sensory neurons ALM and PVD are not taken into account):

- 100% of gap are required
- 62.16% of inhibitory synapses are required in the merged circuit, average number of synapses for one connection are 4.2 synapses
- 95.52% of excitatory synapses are required in the merged circuit, average number of synapses for one connection are 2 synapses
- In summary 80.41% of all chemical synapses is present in the merged circuit. The average number of synapses for one connection, which is not present are 3.69 synapses.

If the not-used sensory neurons are not taken into account, 1/5 of all the chemical synapses are not strictly required in order to process anterior and posterior tap stimulus correctly. The missing connections are relatively weak with the average number of synapses 4.2 for the inhibitory and 2 for the excitatory synapses. The excitatory synapses are supposed to be more important than inhibitory synapses, because 95.52% of all excitatory synapses are present in the required circuit compared to the 80.41% of necessary inhibitory synapses. All of the gap junctions are present in the merged circuit suggesting a big importance of electrical coupling within the circuit.

The role of synapses which have not been presented in the merged TW circuit may be subjected to the future research. Similar to the experiment on Figure 4.14D, the missing connection may modulate the voltage levels to get closer to the scenario where no synapse nor neuron is ablated. Furthermore, we can assume the missing connections as the trace of robustness of the circuit providing a parallel (probably weaker) signal propagation. The parallel pathways are potentially utilized when some of the crucial connection is disrupted. Another role of weak synapses could be the learning process.

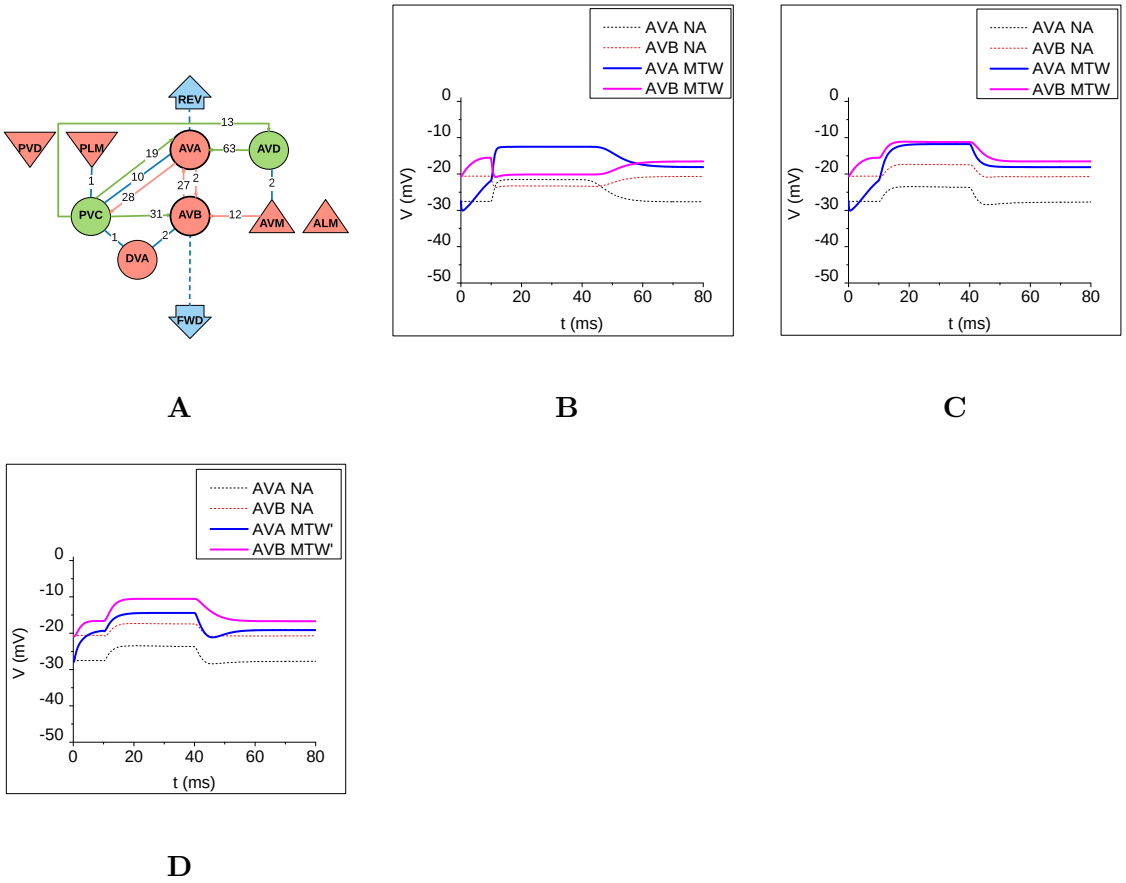

Figure 4.14: **Merging of the backward- and forward-responsible minimal TW circuits. (B-D)** Comparisons of voltage traces for anterior and posterior tap stimuli for complete TW circuit and the merged circuit. AVA and AVB membrane potentials are displayed with the black and red dashed lines, respectively. The anterior tap is applied to the AVM and posterior tap to the PLM sensor neurons. **(A)** The model of merged TW (MTW) circuit for anterior and posterior tap processing (Figures 4.6U and 4.12Q). The inhibitory synapses are displayed with the red, excitatory with the green and gap junction with the blue color. **(B)** Anterior tap stimulus applied to the merged TW circuit. The circuit recognizes the start and end of the stimulation and supports the default forward crawling when no stimulus is applied. **(C)** Posterior tap stimulus applied to the PLM sensor neuron. Again, the circuit is able to respond on the begin and end of the stimulus period and AVB command interneuron, responsible for the forward locomotion, is activated more than AVA neuron. The AVA membrane potential is relatively high compared to the complete TW circuit. **(D)** The high activation of AVA from the C figure can be avoided by adding the inhibitory synapses PLM-AVD and PLM-AVA, which decrease the excitation from AVD interneuron during the stimulus event. MTW' holds form merged TW circuit extended by the inhibitory synapses PLM-AVD and PLM-AVA.

4.4 Comparison of theoretical results with biological experiments data

It is important to validate the results of the theoretical analysis with the generated experimental data on real systems. One source of deviation between "computer" ablations and laser ablations could be that the modeled TW circuit is taken out of context of the remaining neurons within the C. elegans neuronal network. The experimental data was assessed by measuring the response of the real worm to the tap stimulus, so entire neuronal network was taken into account in that case.

Experimental data on the impact of neuronal ablation to the reverse movement was measured by Wicks et. al in 1995 [9]. Reversal frequency together with acceleration and response magnitude were measured by segmenting the trace and velocity of the stimulated nematode. The acceleration magnitude describes the change of velocity in the specific direction of movement, the response magnitude is the length of the trace. Reversal magnitude is the response magnitude as a percentage of the worm's body length and the frequency stands for the number of animals responded with a given response type [9]. In our experiment, we use the Equation 3.5 to measure the direction of locomotion, where it is assumed a proportion between the depolarization of the AVA and AVB neurons and the movement magnitude. Therefore, the empirical data could not be directly compared with the theoretical data. We compare the relative changes of the magnitude in empirical results with the time change in our theoretical results [2]. Second, in the biological experiments response to touch stimulus has been measured, but the TW circuit used in our theoretical experiments [2] has been modelled according the data retrieved by investigating on tap stimulus.

The following Table 4.5 compares the theoretical model with the empirical experiments [9]. The first row contains the values for the circuit without any ablation and in the following rows, this values are compared to the neuron ablations scenarios. The change is assessed relatively by percentage. To recall the difference between the units in theoretical and biological models, we are using the time in milliseconds to state, how long did the C. elegans moved backward in the theoretical model. The biological model is based on reversal magnitude, which is the percentage of the length of the trace moved backward to the length of the worm's body. Both δs are evaluated regarding their positive or negative value, green and red background color are used respectively. The missing value in the biological data when the ALM neuron is ablated is because of this neuron was always ablated together with some other neuron in the reversal magnitude analysis. But in each of these group ablation, the reversal magnitude decreased, therefore we can assume, the ALM ablation has negative impact on the reverse locomotion.

By comparing the corresponding δs, three rows (PLM-, PVC- and PVD-) have different signs of their percentages. Some of the corresponding δs differ quite quite a lot even they both are positive or negative. This inconsistencies arise from expressing relative changes of different measuring units in the theoretical and biological models. We do not quantify the relation between the time spent on reverse movement and the percentage of

	THEORETICAL MODEL		**BIOLOGICAL MODEL** [9]	
Ablated neuron	t [ms]	δ_t [%]	RM [%]	δ_{RM} [%]
NA	34.7	0	62	0
ALM-	32.8	-5.48		
PLM-	34.2	-1.44	108	74.19
AVD-	0	-100	10	-83.87
PVC-	79.8	129.97	49	-20.96
PVD-	41.8	20.46	42	-32.25
DVA-	0	-100	21	-66.12

Table 4.5: **Comparison of theoretical and empirical neuron ablations impacts on reverse locomotion.** The first column specify the ablated neuron or no ablation scenario. The following two columns are the results of our theoretical experiments. The time spent on reverse movement for each ablation was measured and the relative change δ_t was computed as a percentage of the time period spent on reverse locomotion when no neuron was ablated. Similar computations were done for the biological model in the 4th and 5th columns. Instead of time, the reversal magnitude RM and its difference δ_{RM} were assessed [9]. The signs δ_t and δ_{RM} are distinguished by the red background color for negative δ and green background color for positive δ values.

the length of the run to the worm's body. Therefore, the comparison of absolute values of the corresponding δs has not much sense. Furthermore, even the PVC ablation decreases the reversal magnitude in the biological model, the response magnitude and reversal frequency do not change and the worm always reverses [9] which is consistent with the result for PVC ablation in the theoretical model.

The results from the synaptic ablations could not be compared to the biological experiments, as there is no complex research on that. Only few synaptic ablations to investigate the information flow within the circuit [8].

CHAPTER 5

Discussion

Analyzing the results of the experiments, we discovered several principles and mechanisms of signal processing summarized in this chapter.

5.1 Concepts utilized by the merged C. elegans neuronal network

Concepts of the signal propagation and processing in the backward- and forward-responsible and merged circuits, are described in this section.

5.1.1 Gap junctions

Gap junctions are supposed to have two major roles within a neural network. First, they allows the electrical current to pass from the presynaptic to the postsynaptic neuron very fast, second, they synchronize the voltage level of the neurons interconnected by the gap junctions [61]. While the first property is utilized mostly in the neuronal pathways building a reflex reaction to the life endangering stimuli, the second property allows a simultaneous depolarization or hyperpolarization of a group of neuron at the same time [62].

The neuronal circuit of C. elegans contains the gap junctions serving quick feed-forward signal transmission and also the gap junctions synchronizing the voltage level inside the connected neurons. The minimal forward-responsible circuit (Figure 4.12Q) incorporates the PLM-PVC gap junction (Figure 4.12C) to allow the stimulus signal pass from the sensor neuron to the layer of interneurons. It is the single option how to pass the signal, because the sensor neurons are supposed to be inhibitory to their postsynaptic targets [2, 20]. Further, this minimal circuit contains a gap junction pathway PVC-DVA-AVB (Figure 4.12E), which is a synchronization between the two end-points of this pathway –

PVC and AVB, playing an important inhibitory balance, during the steady state, to the excitatory PVC-AVB synapse. Another electrical synchronization is enabled by the strong PVC-AVA electrical coupling, keeping the activation values of AVA and PVC neurons correlated. Because of bi-directional nature of the gap junctions, this synchronization increases to excitatory influence of the PVC-AVA synapse. On the other hand, it decreases the membrane potential of PVC because of AVA-PVC inhibitory synapses, which in turn weakens the PVC-AVB excitation. This complex mechanism is the way how the neuronal network keeps the membrane potentials of AVA and AVB command interneurons correlated to each other.

In the minimal backward-responsible circuit (Figure 4.6U) we also find an evidence of fast signal transmission between the AVM and AVD neurons (Figure 4.6A) and synchronization of the AVA and PVC neurons (Figures 4.6Q, 4.6R). In this circuit, the PVC-AVA synchronization is crucial to make the difference of membrane potentials of AVB and AVA smaller and to enable default forward locomotion before and after the stimulus is applied.

5.1.2 Chemical synapses

The inhibitory or excitatory nature of the chemical synapses and the number of synaptic connections are supposed to build the logic of the neuronal network [61], [62]. While the gap junctions only transmit the signal or synchronize the voltage level among connected neurons, the structure of chemical synapses determines the decision making on which and how much the neurons will be activated or not.

Gain control

The neuronal ablations emphasize the excitatory neuron for each of the two minimal circuits. These neurons take a gain to activate the appropriate command interneuron [2], [20]. For the backward-responsible minimal circuit, it is the AVD neuron activating by 763 excitatory synapses the AVA neuron. Similar for the forward-responsible minimal circuit, the PVC interneuron is resposible for taking gain for initiating the AVB neuron and by that promote forward locomotion.

Behavioral concurrency

It it assumed, that the command interneurons behave as a bistable switch [5] in order to promote only one of the opposite behavioral outputs. If one command neuron, responsible for specific behavioral output, is activated, the other command interneuron, controlling the opposite behavior, needs to be inhibited. From the perspective of computation, this principle is called Winner-take-all [63]. Several different mechanisms could be found within C. elegans neuronal network supporting the imbalance between opposite behaviors (i) direct cross-inhibition, (ii) concurrent activation and (iii) indirect cross-inhibition. The third one was not revealed in the time and voltage analysis of the TW circuit, because it is based on the neurosecretory neurons, disabling parts of the network indirectly be

releasing specific neurotransmitters or neuromodulators [64]. The concurrent activation could be observed by the stimulation of the posterior PLM sensor. Both, AVA and AVB command interneurons are activated simultaneously 4.9, the more activated neuron takes control of the movement [2]. Because the forward locomotion is the default direction during free run, the posterior tap stimulus does not need to outperform the backward circuit.

The direct cross-inhibition, observed during the anterior tap stimulus event 4.3, is probably the most expected way, how to handle concurrency within the circuit. The AVM sensor neuron directly inhibits the AVB command interneuron. Similar procedure would be expected also in forward-responsible circuit because of the inhibitory synapses PLM-AVA and strong AVB-AVA inhibition. But the voltage analysis of the TW circuit showed, that this inhibition is outperformed by the PVC-AVA excitation, resulting not in cross-inhibition but in concurrent activation. In comparison to the concurrent activation, in the case backward withdrawal, the backward-responsible circuit has to beat the by default, more supported, forward-responsible circuit. To this end, the forward circuit is inhibited to allow the AVA activation win over AVB.

5.1.3 Detection of the start and end of stimulation event

By building the minimal forward and backward circuits from scratch (Figures 4.6A – 4.6V, 4.12A – 4.12R) we observed mechanisms to allow the command interneurons to recognize the start and end of the tap stimulus.

Start of the stimulus

The simplest way how to recognize the start of the stimulation is the gap junctions pathway from the sensor to the interneuron observed in PLM-PVC and AVM-AVD couplings. In case of only excitatory synapses from the corresponding excitatory interneuron PVC or AVD to the command interneuron, the stimulus could not be recognized because the target neuron, because its membrane potential will converge to the resting potential of the excitatory chemical synapse (Figures 4.6Bb and 4.12D) right after the start of the simulation. This avoid this situation, the excitatory synapse need to be balanced during the steady state, either by inhibition of command neuron (Figures 4.6G, 4.6H) or by inhibition of command neuron together with inhibition of corresponding excitatory neuron (Figures 4.12G, 4.12H). The inhibition is done either by inhibitory chemical synapses, or by gap junctions, which have inhibitory effect during the steady state, if at least one of the connected neurons is supposed to be inhibitory.

End of the stimulus

When the tap stimulus is over, there is no further stimulus current depolarizing the sensor neuron and coupled excitatory neuron (PVC or AVD), but because of the nature of electrical synapses, the repolarization in this couple is significant slower compared to the repolarization of chemical synapse. Slow depolarization of excitatory interneuron

causes the membrane potential of command neurons to not decreasing after the end of stimulus (Figure 5.1B). To enable the correct repolarization in the post-stimulus phase, the sensor-interneuron couple need to be inhibited. In case of forward-responsible circuit, the PLM-PVC coupling is balanced by the AVA-PVC inhibitory synapse, which causes a repolarization after the stimulus is over. Similar mechanism can be observed in the backward-responsible circuit where in difference to previous case, the inhibition of AVD interneuron is caused by the excitatory synapse PVC-AVD (Figure 5.1D). The PVC interneuron does not receive any activation during the anterior tap stimulus, so its membrane potential is closed to the resting potential and therefore even then excitatory synapse has an inhibitory effect on high-depolarized AVD interneuron.

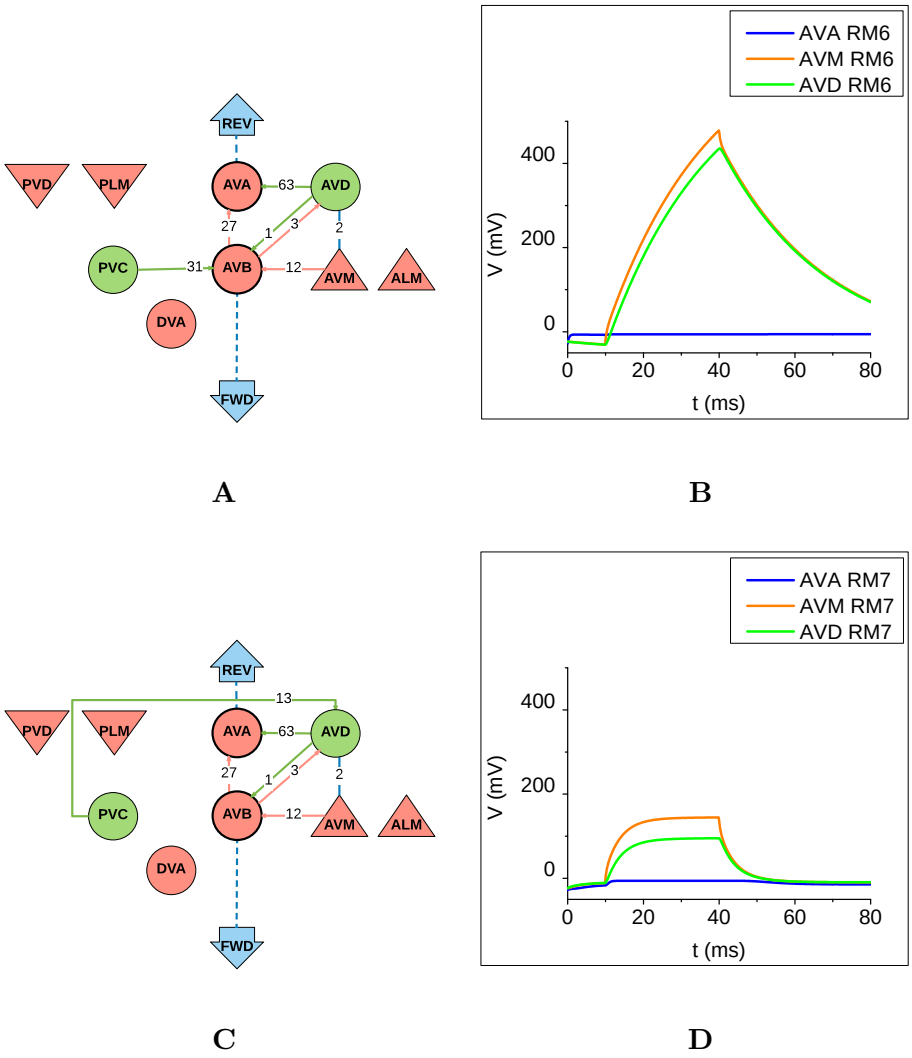

Figure 5.1: **Recognizing the end of tap stimulus by AVD interneuron. (A-B)** Model of TW circuit from building of forward-responsible minimal circuit (Figure 4.6K). The depolarization of AVD (green) after the end of stimulus is slow because of missing inhibition of electrical coupling with AVM (orange). AVA neuron (blue) is not able to recognize the end of the tap stimulus. **(C-D)** Model of TW circuit from building of forward-responsible minimal circuit (Figure 4.6M). The depolarization of AVD is controlled by the inhibitory impact of 13 excitatory synapses from repolarized PVC neuron. AVA is able to recognize the end of the tap stimulus.

5.1.4 Cycles within the circuit

The building of the neural circuits from scratch revealed cycles necessary for correct processing of the tap stimulus. We define a cycle as a pathway of chemical synapses, where the starting and ending neurons are the same. For instance, A-B-C is a cycle

with chemical connections A-B, B-C and C-A. Three cycles were discovered within the minimal forward- and backward-responsible circuits.

AVA-PVC-AVB cycle

This cycle (Figure 5.2A) is present in both, forward- and backward-responsible minimal circuits. If we separate this cycle from all outgoing and incoming synapses from the uninvolved neurons, the cycle polarizes its neurons into two groups, in the way that AVA and PVC membrane potentials converge to the reverse potential of inhibitory synapse and on the other hand, the AVB membrane potential will converge to the 0 mV, which is a reverse potential of excitatory synapse. The cycle negatively correlates the activations of AVA and AVB. Therefore, the command interneurons responsible for the forward and backward locomotion are mutually inhibited by this cycle in favor of forward locomotion. We can assume this cycle as one of the supportive mechanisms to support the default forward locomotion, discussed in Section 3.2. In the minimal forward-responsible circuit, adding this cycle initiate the AVA command interneuron to recognize the stimulus event as well as to keep the AVA activation lower than AVB activation (Figures 4.12O, 4.12P). In the minimal backward-responsible circuit the AVA-PVC-AVB cycle helps to balance the excitatory synapse AVD-AVA and inhibitory synapse AVM-AVB in order to recognize the start of the stimulus event (Figures 4.6S, 4.6T).

AVA-PVC-AVD cycle

Next cycle (Figure 5.2B) was discovered by building of the backward-responsible minimal circuit. Isolated cycle behaves in favor of the backward locomotion through AVD and AVA activation and PVC deactivation, which is the control neuron for forward movement. Therefore, it has an opposite role to the AVA-PVC-AVB cycle, but it also incorporates the forward and backward related neurons. Adding the synapses and gap junction of backward-responsible circuit, this cycle is supposed to play against the AVM-AVD electrical coupling to control the depolarization of AVD. The repolarization of AVD is necessary in order to recognize the end of the stimulus by AVA and AVB command interneurons. Both cycles, AVA-PVC-AVB and AVA-PVC-AVD, overlaps each other with the AVA-PVC inhibitory synapse, which causes the PVC deactivation in both cycles. When the stimulus current reach the two excitatory neurons AVD or PVC, one of the cycles takes the control of activation and deactivation of the command interneurons AVA and AVB.

AVA-PVC cycle

Following cycle consists of only two neurons, which is a minimal precondition on existence of a cycle (Figure 5.2C). Between the neurons AVA and PVC are all three types of synapses - gap junctions, inhibitory and excitatory synapses. The cycle, free of any incoming synapse from uninvolved neurons hyperpolarizes PVC interneuron and depolarizes AVA command neuron. During the stimulation of PLM, PVC becomes activated and controls

its activation through AVA neuron, by supporting its inhibitory impact through 19 PVC-AVA excitatory synapses. The AVA-PVC synapses are important to force the PLM-PVC electrical coupling to quicker repolarize after the stimulation is done. In summary, this cycle has a twofold role: (i) co-activate AVA neuron and (ii) control the PVC depolarization in the steady state.

AVA-AVB cycle

Similar two-component cycle to the AVA-PVC. In difference to the previous cycle, both of the involved neurons – AVA and AVB – are supposed to by inhibitory (Figure 5.2D). The function of such a circuit is the mutual inhibition of the connected neurons. Because of higher number of AVB-AVA synapses compared to the opposite AVA-AVB synapses, the AVA receives much stronger inhibition an its inhibitory impact on AVB is significantly weaker. This imbalance support the default higher activation of AVB and by that the default forward crawling.

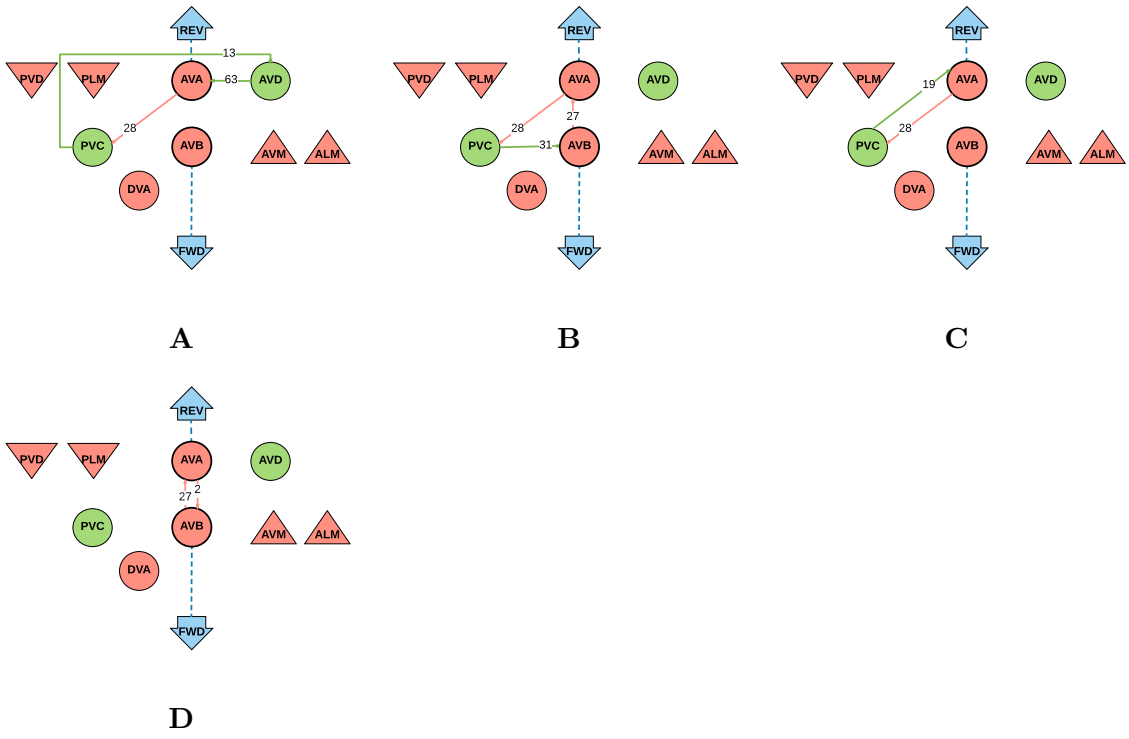

Figure 5.2: **Functional cycles within the merged TW circuit. (A)** Cycle AVA-PVC-AVB taking importance in both backward- and forward-responsible minimal circuits.**(B)** Cycle AVA-PVC-AVD is necessary for correct propagation of backward locomotion. **(C)** Cycle composed of one excitatory (PVC) and one inhibitory neuron (AVA). This cycle activates AVA neuron and control the PVC depolarization by the AVA-PVC inhibition. **(D)** Mutual inhibition of the command interneurons AVA and AVB. The imbalance in the number of synapses supports the default forward locomotion.

5.1.5 C. elegans neuronal network architecture

Investigating the C. elegans neural network responsible for tap withdrawal, the neurons can be divided into four functional groups. The impulse from the external environment is sensed by the sensor neurons (ALM, AVM, PLM and PVD) and through electrical synapses passed to the layer of interneurons (AVD and PVC). Further, the output of the interneurons is transmitted using mostly chemical synapses to the command interneurons (AVA and AVB), which are electrically connected to the motor neurons communicating directly with muscles of the body. We can name the layers from top to bottom *Sensory layer*, *Control layer*, *Command layer* and *Motor layer* (Figure 5.3).

Comparing this architecture with the other neural circuits responsible for chemotaxis and thermotaxis [5, 18], we are able to confirm the four layers and extend the knowledge about the modules of the entire nervous system. For each behavioral output like tap withdrawal, thermotaxis, chemitaxis etc. there are separate sensor neurons, sensing the specific type of stimulus (there are also polymodal sensors to sense different classes of stimuli [58, 8]). Sensor layer of each of the bahavioral activity binds to the control layer, specific for the single behavioral activity, too. But as far as most of the C. elagans' answers to the different stimuli is either forward or backward locomotion, the command layer is shared by all of the control modules. Therefore also the motor neurons are common for all of the different behavioral activities.

Data transmission and interpretation is ensured by the electrical and chemical synapses and by the number of these connections. Sensor layer binds unidirectional to the control layer with chemical synapses and bidirectional with gap junctions. It also express chemical connectivity to the command layer (for instance AVM-AVB) and motor layer (AVM-DA), which both are rather rear scenarios. The gain control procedure (Section 5.1.2) is performed in the control layer, which is synaptic connected to the command and motor layer in both directions. In some specific scenarios, there are also electrical synapses between the control and command layer, for instance AVA-PVC electrical coupling. The command layer builds a strong gap junctions to the motor layer to activate the motor neurons. These two layers exchange the electrical current between each other also using the chemical synapses in both directions. The decision on forward or backward locomotion is not made within a single layer, it is taken by involving the first three layers. The sensor layer is the only layer not targeted by any chemical synapse, but it has a chemical connections to all three remaining layers, which means that the input signal from the sensory neurons is integrated to all of the other layers, but only the control layer is able to synchronize its state with sensor layer via gap junctions.

The direct connections between two non-neighboring layers may suggest a backup pathways to control the locomotion even the control or command layer is missing or heavily disrupted. It makes the nervous system robust and fault tolerant.

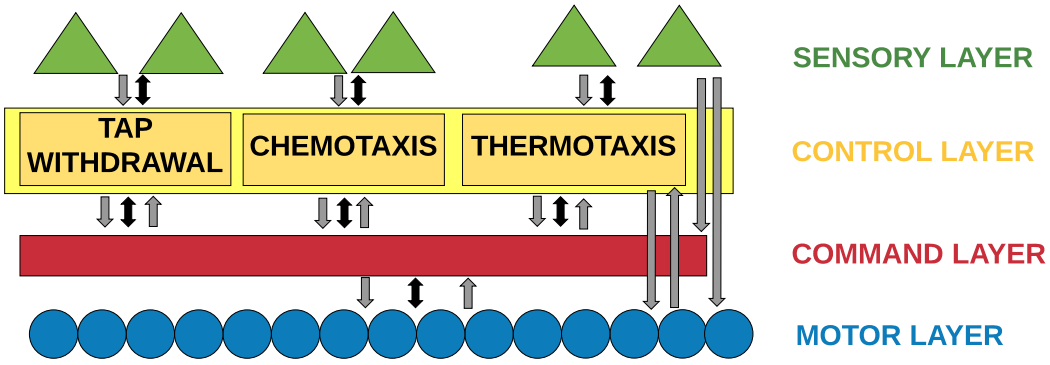

Figure 5.3: **Architectural model of the C. elegans neuronal network.** The sensory layer is depicted with the groups of the green triangles, responsible for sensing specific type of stimulus. Control layer, displayed with the yellow box, is a set of modules, each of the module is dominant for one behavioral activity. The command layer – red box – is shared by all of the controlling modules. Finally, the motor layer is depicted with the blue circles. The gap junctions are displayed with the black bidirectional arrows, while the chemical synapses are drawn with unidirectional arrows.

5.1.6 Parallels of the C. elegans neuronal network concepts to the distributed controller in computer science

This section provides a translation of the previously described concepts to the computer science language. Particularly, the "brain" behind the locomotory behavior and the concepts used within this nervous system are equivalent to the architecture of distributed controller in computer science, where each group of specific tasks is controlled by separate controller communicating each other in order to cooperate their actions.

Let's assume a boat equipped by the controller module performing the autopilot functionalities. From the higher perspective, similar to C. elegans, this autopilot receives information about the external environment through the sensors (for instance light, temperature sensor, radar), process this information in a specific way sends the commands (break, full gas, turn left) to the actuators. Actuators are equivalent to the motor neurons connected directly to the muscles.

The gap junctions are either used to transmit the signal from one functional layer to another or to synchronize the voltage level across multiple neurons. In our autopilot example the messaging routes between the components of the controller and the shared space where the modules share their internal states are the parallels to the electrical coupling within the neuronal network.

In the situation when GPS sensor on the boat suggests the autopilot to take a right turn and for example the wind sensor prefers to turn left, two concurrent processes want to access the turning actuator. This is a similar scenario to the co-activation of both AVA and AVB command interneurons and the winner is determined by the several mechanisms

in the network discussed in the Section 3.2. The autopilot also implements policies to decide what process takes the control of the actuator when multiple concurrent processes try to access it. This could be for example locking mechanism on the utilized actuator when it is in use. Basically, the business logic of the autopilot controller expressing the way how the signal data is processed and evaluated is the alternative to the number, polarity and both end-points of the synapses.

We are able to map the concepts of the C. elegans neuronal network to the autopilot controller which leads to an assumption that the neuronal network works on principles of distributed controller built upon neurons as the controlling units, grouped into functional layers, communicating each other and expressing the logic through electrical and chemical synapses, cycles, feedback loops etc.

CHAPTER 6

Future work

TW circuit as a NC receives an stimulus signal by the sensor neurons, process it and transforms it into command for the motor neuron. Equivalent workflow is required by large variety of controlling systems including medicine, industry, finance etc. The acquired knowledge about the basic operational principles of TW circuit is demonstrated on simple decision module driving stock market investor.

The value of stock is represented by its price in specific point of time. Stock market is a dynamic environment, with numerous price-impacting factors. The main goal of an investor, trading on stock market, is to gain possible highest value for their assets. To this end, investors use different indicators to predict the situation on the market and take the appropriate position in order to increase the value of their assets. For example, indicator called Moving Average (MA) filters the noise of the prices by taking and weighting the historical values to predict the near-future situation [65]. Based on the analysis of indicators, investor decides on buying or selling (shorting) stocks, or he will take no action.

TW circuit is able, according to the stimulated sensor neuron, promote one of the opposite behavioral actions – forward and backward locomotion. We can map the time-specific indicator values to the input signal, the signal processing by interneurons to evaluation of indicator values and the commands to the taking BUY or SELL action. In our solution, we assume the current value $I(t)$ and the last historical value $I(t-1)$ of the indicator. Based on the comparison of these values, the decision on BUY or SELL of stocks in undertaken (Equation 6.1). The δ is a recognize threshold for SELL action, indicating the minimal difference between the current and historical value to trigger SELL action. The value of δ was measured by experiments and it is close to 0.2 nA.

$$\begin{aligned} I(t) > I(t-1) + \delta &\rightarrow \text{ SELL} \\ I(t << I(t-1) &\rightarrow \text{ BUY} \\ I(t) - I(t-1) \leq \delta &\rightarrow \text{ nothing} \end{aligned} \tag{6.1}$$

Greater current value of the indicator compared to the historical value indicates the SELL action. If the current value is lower or than historical value, investor take the BUY position. If the difference between the values of indicator is less than recognize threshold, indicating the unchanged situation on the market, no action is taken.

The wiring model of the Indicator evaluation module consists of 8 neurons building synaptic and electric connections based on the principles of TW circuit (Figure **??**A). The current value of indicator is passed to the CRT sensor neuron and the historical indicator value is inserted into HST sensor neuron. The role of the interneurons is to compare the current value with the historical value. Each of the input signals is passed to one excitatory and one inhibitory neuron indicating *plus* and *minus* sign for each value. In the next step, the difference between the current and historical indicator values and the opposite difference between the historical and current values, are computed by the interneurons CHD and HCD, respectively. Because of mutual inhibition between CHD and HCD neurons, the bigger value wins over the lower value of indicator and activates corresponding sensor neuron in the C. elegans TW module. Th TW module is a full copy of merged backward- and forward-responsible minimal circuits from the Section 4.3. The AVA response is triggering the SELL action and the AVB activation controls the BUY action.

The number of connections in the Indicator evaluation module has been set manually by experiments. Because of default higher activation of AVB, compared to the AVA, the signal passed to the AVM sensor neuron has to be stronger to outperform AVB. To this end, we use different numbers of connections for the gap junctions from CRT, HST sensor neurons and corresponding interneurons. To control the activations of the pairs of inhibitory-excitatory neurons (HSA-HSS and CRA-CRS) we use similar controlling cycles as PVC-AVA neurons in the TW circuit. Moreover, the HSS and CRS inhibitory neurons, responsible for subtraction of indicator values, are mutually inhibited to emphasize the difference between current and historical value of indicator. Finally, the computation of difference is performed by HCD and CHD neurons receiving the positive impact of current indicator value and negative impact of historical value and vise versa, to determine which of these differences has a positive value to stimulate corresponding sensor neuron of TW circuit (Figure **??**B).

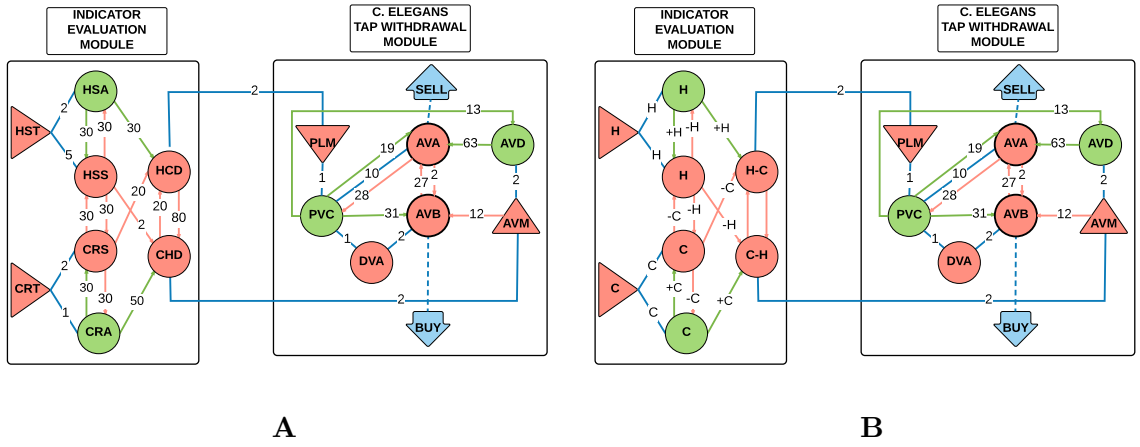

Figure 6.1: **Wiring model of simple decision module for stock market investor. (A)** The decision module is composed of two sub-modules – Indicator evaluation module and C. elegans tap withdrawal module. The current and historical values of the indicator are passed to the sensor neurons (CRT, HST) and the values are compared with the help of 6 interneurons. The result of the comparison is forwarded to the sensor neurons of TW circuit (AVM, PLM). TW circuit process the signal in the same way as the tap stimulus and the output of command interneurons is interpreted as the stock market actions – SELL and BUY **(B)** The arithmetic behind the structure of Indicator evaluation module. The current value of indicator (C) and historical value (H) are passed through the gap junctions to one inhibitory and one excitatory interneuron for each of the values. The subtraction H-C is computed in the HCD neuron and the inverted subtraction C-H is performed by the CHD neuron. This mechanisms ensures that only one of the CHD and HCD neurons is depolarized to trigger corresponding sensor neuron of the TW circuit.

The physiological properties for the neurons of Indicator evaluation module are equal to the values for neurons of TW circuit. The membrane capacitance and resistance of the sensor neurons HST and CRT are equal to the values of AVM sensor neurons. The membrane properties interneurons has been adopted from the AVA neuron.

Table 6.1: Table of neuron names for investor decision module.

Shortcut	**Long name**
HST	Historical value of indicator
CRT	Current value of indicator
HSA	Historical value add
HSS	Historical value subtract
CRA	Current value add
CRS	Current value subtract
HCD	Historical-current difference
CHD	Current-historical difference

The NC for the stock market is examined by the series of experiments with different values for the indicator (Figures 6.2A, B). We applied 50 ms pulses of different intensity to the HST and CRT sensor neurons to check the decision of the NC. The logic behind the intensities of pulses is to check all possible combinations of two pulses in a row. First two pulses have an increasing trend of indicator value, indicating the SELL action. During the following two pulses, the current value of the indicator decreases, implying the BUY action. In the next two pulses, the indicator value increases first and then decreases again, to check the response on immediate change in trend of indicator values. In the last pulse, we applied stimulus greater than the previous value, but lower than recognize threshold δ, so the circuit responds with no action (Eq. 6.1).

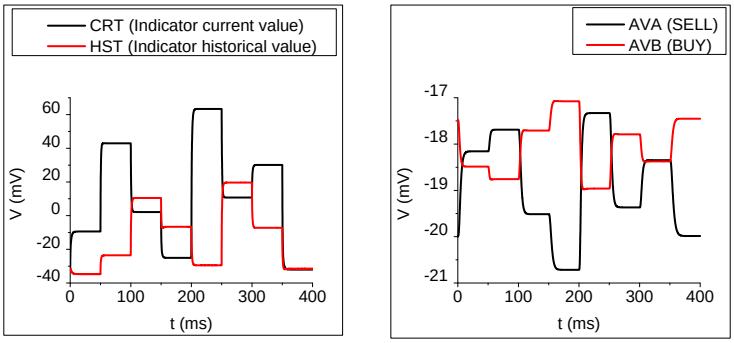

A **B**

Figure 6.2: (Previous page.) **Decision making of stock market investor based on the current and historical values of chosen indicator. (A)** The input values for the indicator are mapped to the electrical current. We generate 7 different pulses with duration of 50 ms for the current value of indicator (black line). The historical value (red line) is the previous value of indicator. The first two intervals generate increasing value for indicator, followed by the two intervals with decreasing indicator value. Next, the indicator value is increased for one pulse and then decreased for one pulse, again. In the last interval, the difference between the current and historical value is less than recognize threshold δ. The voltage of HST sensor neuron is not copy of the last voltage of CRT neuron, because of different number of gap junctions between the sensors and related interneurons. **(B)** The decisions of the investor on buying (red line) or selling (black line) stocks. If the current value of indicator is greater than the historical value on the graph A (1st, 2nd and 5th pulse), AVA (SELL) neuron is activated while AVB neuron (BUY) is inhibited. Opposite behavior can be observed in case of higher historical value of indicator compared to the current value (3rd, 4th and 6th pulse), where the BUY action is taken. During the 7th pulse, the difference between the current and historical value of indicator is lower than recognize threshold δ, AVA is not able to outperform AVB neuron to initiate SELL decision. The circuit promotes BUY action as a default decision, similar to the default forward locomotion of C. elegans, when no stimuli are applied to the HST, CRT sensors.

We were able to construct a neuronal module composed of the neurons of TW circuit, working on similar principles as NC controlling the tap withdrawal behavioral action. The indicator evaluation module is able to perform simple arithmetic, which is a promising step for building more complex logic. Based on the different values of indicator, the module decides on appropriate action. In the future research, more indicators may be taken into account and evaluated based on the more complex logic as only simple comparison.

CHAPTER 7

Conclusion

In this research activity, we extracted novel neuronal control principles by investigating the locomotory neural circuit of the worm C. elegans. By performing synaptic ablations, we identified the crucial synaptic and electric connections which build the signal forwarding and processing. For this purpose, we investigated the time spent on the forward or reverse locomotion after injection of a tap stimulus. As it turned out, the initiation of the reverse locomotion is bound with the inhibition of forward-responsible circuit. Therefore, there are two crucial pathways for backward withdrawal – gaining the control of backward responsible interneuron AVA and suppression of forward circuit. In case of forward tap withdrawal, both of the opposite circuits are activated, but because of intrinsic bias towards forward locomotion as a default locomotory output, and the mutual inhibition of AVB, the activation of forward responsible command interneuron AVB is higher than AVA. The robustness of TW circuit has been proven by reducing or removing synaptic connections while preserving the expected behavioral output.

The role of single synapses and functional cycles are demonstrated by building of forward- and backward-responsible minimal circuits from scratch. We identified several tasks, that need to be accomplished in order to get the correct answer in terms of activation/deactivation of AVA and AVB. The corresponding excitatory neuron has to be activated in order to gain control of the expected command neuron activation. On the other hand, the excitatory neuron requires simultaneous inhibition, in order to repolarize after the tap stimulus is over. the concurrency between opposite circuits is ensured by mutual inhibition or co-activation with the bias towards the expected command neuron. Gap junctions play important role in the fast signal transmission from sensor neurons to the interneurons and to synchronize the voltage level of connected neurons.

We also examined the modularity and possible interference of the forward- and backward-responsible minimal circuits by merging them into one NC. The resulted circuit is able to respond with the correct withdrawal to both, anterior and posterior tap stimuli. This implies an assumption, that the overall neuronal circuit, despite high rate of

interconnectivity can be decomposed into smaller circuits governing only one behavioral output.

In the final step, the decision module for stock market trading investor has been designed based on the extracted principles utilized by the TW circuit. With the C. elegans equivalent neurons, we demonstrated implementation of simple arithmetic operation by comparing the current and historical values of chosen stock market indicator, suggesting the investor to BUY or SELL stocks. Such a adaptation of BNN in different controlling scenario may suggest a new fashion in design of NC.

List of Figures

List of Tables

List of Algorithms

Appendix

All TW simulations has been performed by extended version of Matlab scripts [44]. The source code is available in github
https://github.com/ondrejbalun/ondrej_balun_master_thesis_celegans.git.

Model properties

- *Connectivity_matrix.mat* – TW circuit wiring model.
- *Connectivity_matrix_simple_investor2.mat* – Investor decision module circuit wiring model.
- *InitialState.mat* – Initial setup of TW neurons
- *InitialState_simple_investor2.mat* – Initial setup of Investor decision module neurons

Simulations

- *mainTWSimulation.m* – Simulates the tap withdrawal and computes the time spent on forward and backward locomotion when tap stimulus applied (used for synaptic ablations).
- *ablations.m* – Performs ablations of synapses and checks the time difference.
- *mainTWSimulation_neuron_ablation.m* – Simulates the tap withdrawal and computes the time spent on forward and backward locomotion when tap stimulus applied (used for neuronal ablations).
- *neuron_ablations.m* – Performs ablations of neurons and checks the time difference.
- *VoltageTraces_mainTWSimulation.m* – Simulates the tap withdrawal and collect the membrane potentials of neurons during simulation (used for synaptic ablations).
- *VoltageTraces_ablations.m* – Performs ablations of synapses and checks the voltage traces.

- *VoltageTraces_mainTWSimulation_neuron_ablations.m* – Simulates the tap withdrawal and collect the membrane potentials of neurons during simulation (used for neuronal ablations).
- *VoltageTraces_neuron_ablations.m* – Performs ablations of neurons and checks the voltage traces.
- *simple_investor_Simulation.m* – Simulates the investor on stock market and collect the membrane potentials of neurons during simulation.
- *VoltageTraces_investor.m* – Prints the voltage traces of investor neurons to file.

Model utils

- *TWModel_dynamics.m* – ODE function for TW circuit.
- *newNeuronID.m* – Computes new neurons IDs when neuronal ablation applied.

Datasets

- */datasets/AVM_stimuli/gap_junctions/* – Voltage traces of AVA and AVB neurons during synaptic ablations, when applying anterior tap
  (file name format: voltage_traces_g_AVM_stim_<id_of_presynaptic_neuron>_<id_of_postsynaptic_neuron>_<how_many_synapses_ablated>_<out_of_how_many_synapses>.txt).
- */datasets/AVM_stimuli/synapses/* – Voltage traces of AVA and AVB neurons during synaptic ablations, when applying anterior tap
  (file name format: voltage_traces_s_AVM_stim_<id_of_presynaptic_neuron>_<id_of_postsynaptic_neuron>_<how_many_synapses_ablated>_<out_of_how_many_synapses>.txt).
- */datasets/AVM_stimuli/time_changes.txt* – Time changes of forward and backward locomotion during synaptic ablations, when anterior tap stimulus applied.
- */datasets/AVM_stimuli/voltage_traces_no_ablation_AVM_stim_.txt* – Voltage traces of AVA and AVB neurons during synaptic ablations, when anterior tap stimulus applied.
- */datasets/PLM_stimuli/** – Same datasets as for AVM stimulus, but for the posterior tap
- */datasets/neuron_ablations/AVM_stimuli/* – Voltage traces of AVA and AVB neurons during neuronal ablations, when applying anterior tap
  (file name format: <id_of_ablated_neuron>_avm_missing.txt).

- */datasets/neuron_ablations/PLM_stimuli/* – Voltage traces of AVA and AVB neurons during neuronal ablations, when applying posterior tap (file name format: <id_of_ablated_neuron>_avm_missing.txt).

Bibliography

[1] H. Haghighi, F. Abdollahi, and S. Gharibzadeh, "Brain-inspired self-organizing modular structure to control human-like movements based on primitive motion identification," *Neurocomputing*, vol. 173, pp. 1436–1442, 2016.

[2] S. R. Wicks, C. J. Roehrig, and C. H. Rankin, "A dynamic network simulation of the nematode tap withdrawal circuit: Predictions concerning synaptic function using behavioral criteria," *The Journal of Neuroscience*, vol. 16, no. 12, pp. 4017–4031, 1996. [Online]. Available: http://www.jneurosci.org/content/16/12/4017.abstract

[3] M. Chalfie, J. Sulston, J. White, E. Southgate, J. Thomson, and S. Brenner, "The neural circuit for touch sensitivity in caenorhabditis elegans," *The Journal of Neuroscience*, vol. 5, no. 4, pp. 956–964, 1985. [Online]. Available: http://www.jneurosci.org/content/5/4/956.abstract

[4] J. G. White, E. Southgate, J. N. Thomson, and S. Brenner, "The structure of the nervous system of the nematode caenorhabditis elegans," *Philosophical Transactions of the Royal Society of London B: Biological Sciences*, vol. 314, no. 1165, pp. 1–340, 1986.

[5] E. L. Tsalik and O. Hobert, "Functional mapping of neurons that control locomotory behavior in caenorhabditis elegans," *Journal of neurobiology*, vol. 56, no. 2, pp. 178–197, 2003.

[6] Y. Zheng, P. J. Brockie, J. E. Mellem, D. M. Madsen, and A. V. Maricq, "Neuronal control of locomotion in c. elegans is modified by a dominant mutation in the glr-1 ionotropic glutamate receptor," *Neuron*, vol. 24, no. 2, pp. 347 – 361, 1999. [Online]. Available: http://www.sciencedirect.com/science/article/pii/S0896627300808491

[7] S. Kato, H. S. Kaplan, T. Schrödel, S. Skora, T. H. Lindsay, E. Yemini, S. Lockery, and M. Zimmer, "Global brain dynamics embed the motor command sequence of caenorhabditis elegans," *Cell*, vol. 163, no. 3, pp. 656–669, 2015.

[8] B. J. Piggott, J. Liu, Z. Feng, S. A. Wescott, and X. S. Xu, "The neural circuits and synaptic mechanisms underlying motor initiation in c. elegans," *Cell*, vol. 147, no. 4, pp. 922–933, 2011.

[9] S. R. Wicks and C. H. Rankin, "Integration of mechanosensory stimuli in caenorhabditis elegans," *The Journal of neuroscience*, vol. 15, no. 3, pp. 2434–2444, 1995.

[10] S. Wicks and C. Rankin, "Recovery from habituation and habituation of spontaneous behavior in c. elegans: dependence on circuit characteristics," in *Society for Neuroscience Abstracts*, vol. 21, 1995, p. 1455.

[11] S. H. Chung, L. Sun, and C. V. Gabel, "In vivo neuronal calcium imaging in c. elegans," *Journal of visualized experiments: JoVE*, no. 74, 2013.

[12] E. R. Kandel and J. H. Schwartz, "Molecular biology of learning: modulation of transmitter release," *Science*, vol. 218, no. 4571, pp. 433–443, 1982.

[13] D. H. Hall, T. Boulin, M. Volaski, M. Zhang, C. Polydorou, and Z. F. Altun, "Wormatlas: A web-based behavioral and structural atlas of c. elegans," 2002. [Online]. Available: http://www.wormbase.org/db/misc/paper?name=WBPaper00012319

[14] S. Cook, C. Brittin, D. Hall, and S. Emmons, "The worm wiring project," 2012.

[15] "Sw-worm viewer," http://www.wormatlas.org/SW/SW.php, 2016.

[16] "The wormimage database," http://www.wormimage.org/, 2016.

[17] S. S. Singh, B. Khundrakpam, A. T. Reid, J. D. Lewis, A. C. Evans, R. Ishrat, B. I. Sharma, and R. B. Singh, "Scaling in topological properties of brain networks," *Scientific reports*, vol. 6, 2016.

[18] A. Gordus, N. Pokala, S. Levy, S. W. Flavell, and C. I. Bargmann, "Feedback from network states generates variability in a probabilistic olfactory circuit," *Cell*, vol. 161, no. 2, pp. 215–227, 2015.

[19] M. Chatzigeorgiou, S. Bang, S. W. Hwang, and W. R. Schafer, "tmc-1 encodes a sodium-sensitive channel required for salt chemosensation in c. elegans," *Nature*, vol. 494, no. 7435, pp. 95–99, 2013.

[20] Y. Iwasaki and S. Gomi, "Stochastic formulation for a partial neural circuit of c. elegans," *Bulletin of mathematical biology*, vol. 66, no. 4, pp. 727–743, 2004.

[21] F. Rakowski, J. Srinivasan, P. W. Sternberg, and J. Karbowski, "Synaptic polarity of the interneuron circuit controlling c. elegans locomotion," *arXiv preprint arXiv:1403.5185*, 2014.

[22] T. Kawano, M. D. Po, S. Gao, G. Leung, W. S. Ryu, and M. Zhen, "An imbalancing act: Gap junctions reduce the backward motor circuit activity to bias c. elegans for forward locomotion," *Neuron*, vol. 72, no. 4, pp. 572 – 586, 2011. [Online]. Available: http://www.sciencedirect.com/science/article/pii/S0896627311007914

[23] S. Faumont, T. Lindsay, and S. Lockery, "Neuronal microcircuits for decision making in c. elegans," *Current opinion in neurobiology*, vol. 22, no. 4, pp. 580–591, 2012.

[24] C. R. Palmer and W. B. Kristan, "Contextual modulation of behavioral choice," *Current opinion in neurobiology*, vol. 21, no. 4, pp. 520–526, 2011.

[25] K. S. Chaisanguanthum, H. H. Shen, and P. N. Sabes, "Motor variability arises from a slow random walk in neural state," *The Journal of Neuroscience*, vol. 34, no. 36, pp. 12 071–12 080, 2014.

[26] E. C. Tumer and M. S. Brainard, "Performance variability enables adaptive plasticity of 'crystallized'adult birdsong," *Nature*, vol. 450, no. 7173, pp. 1240–1244, 2007.

[27] P. Horowitz, W. Hill, and I. Robinson, *The art of electronics*. Cambridge university press Cambridge, 1980, vol. 1989.

[28] C. Koch and I. Segev, *Methods in neuronal modeling: from ions to networks*. MIT press, 1998.

[29] J. M. Gray, J. J. Hill, and C. I. Bargmann, "A circuit for navigation in caenorhabditis elegans," *Proceedings of the National Academy of Sciences of the United States of America*, vol. 102, no. 9, pp. 3184–3191, 2005. [Online]. Available: http://www.pnas.org/content/102/9/3184.abstract

[30] W. M. Roberts, S. B. Augustine, K. J. Lawton, T. H. Lindsay, T. R. Thiele, E. J. Izquierdo, S. Faumont, R. A. Lindsay, M. C. Britton, N. Pokala, C. I. Bargmann, and S. R. Lockery, "A stochastic neuronal model predicts random search behaviors at multiple spatial scales in c. elegans," *eLife*, vol. 5, p. e12572, jan 2016. [Online]. Available: https://dx.doi.org/10.7554/eLife.12572

[31] B. Szigeti, P. Gleeson, M. Vella, S. Khayrulin, A. Palyanov, J. Hokanson, M. Currie, M. Cantarelli, G. Idili, and S. Larson, "Openworm: an open-science approach to modeling caenorhabditis elegans," *Frontiers in computational neuroscience*, vol. 8, p. 137, 2014.

[32] B. Alicea, S. McGrew, R. Gordon, S. Larson, T. Warrington, and M. Watts, "Devoworm: differentiation waves and computation in c. elegans embryogenesis," *bioRxiv*, p. 009993, 2014.

[33] "Openworm browser (1.8.0)," http://browser.openworm.org/, 2012–2013.

[34] "c302," https://github.com/openworm/CElegansNeuroML/tree/master/CElegans/pythonScripts/c302, 2014–2016.

[35] "Sibernetic (0.0.3)," https://github.com/openworm/sibernetic, 2014–2016.

[36] "Geppetto (0.2.8)," http://www.geppetto.org/, 2012–2014.

[37] T. Busbice, "The robotic worm," *BioCoder*, pp. 31–35, 2014.

[38] M. Suzuki, T. Tsuji, and H. Ohtake, "A model of motor control of the nematode c. elegans with neuronal circuits," *Artificial Intelligence in Medicine*, vol. 35, no. 1, pp. 75–86, 2005.

[39] T. M. Morse, S. R. Lockery, and T. C. Ferrée, "Robust spatial navigation in a robot inspired by chemotaxis in caenorhabditis elegans," *Adaptive Behavior*, vol. 6, no. 3-4, pp. 393–410, 1998.

[40] R. M. H. O. B. E. M. C. R. G. S. A. S. Md. Ariful Islam, Qinsi Wang, "Probabilistic reachability analysis of the tap withdrawal circuit in caenorhabditis elegans," 2016.

[41] E. B. Hendrickson, J. R. Edgerton, and D. Jaeger, "The capabilities and limitations of conductance-based compartmental neuron models with reduced branched or unbranched morphologies and active dendrites," *Journal of computational neuroscience*, vol. 30, no. 2, pp. 301–321, 2011.

[42] S. Kirkpatrick, "Optimization by simulated annealing: Quantitative studies," *Journal of statistical physics*, vol. 34, no. 5-6, pp. 975–986, 1984.

[43] T. C. Ferree and S. R. Lockery, "Computational rules for chemotaxis in the nematode c. elegans," *Journal of computational neuroscience*, vol. 6, no. 3, pp. 263–277, 1999.

[44] K. Selyunin, D. Ratasich, E. Bartocci, M. Islam, S. Smolka, and R. Grosu, "Neural programming: Towards adaptive control in cyber-physical systems."

[45] "Database of synaptic connectivity of c. elegans for computation," http://ims.dse.ibaraki.ac.jp/ccep-tool/, 2004–2014.

[46] T. Kimata, H. Sasakura, N. Ohnishi, N. Nishio, and I. Mori, "Thermotaxis of c. elegans as a model for temperature perception, neural information processing and neural plasticity," in *Worm*, vol. 1, no. 1. Taylor & Francis, 2012, pp. 31–41.

[47] "C. elegans neural network," http://wormweb.org/neuralnet#c=BAG&m=1, 2009–2014.

[48] J. N. T. Donna G. Albertson, "The pharynx of caenorhabditis elegans," *Philosophical Transactions of the Royal Society of London. Series B, Biological Sciences*, vol. 275, no. 938, pp. 299–325, 1976. [Online]. Available: http://www.jstor.org/stable/2417636

[49] B. L. Chen, D. H. Hall, and D. B. Chklovskii, "Wiring optimization can relate neuronal structure and function," *Proceedings of the National Academy of Sciences of the United States of America*, vol. 103, no. 12, pp. 4723–4728, 2006.

[50] N. Bhatla, R. Droste, S. R. Sando, A. Huang, and H. R. Horvitz, "Distinct neural circuits control rhythm inhibition and spitting by the myogenic pharynx of c. elegans," *Current Biology*, vol. 25, no. 16, pp. 2075–2089, 2015.

[51] A. Rogers, I. Antoshechkin, T. Bieri, D. Blasiar, C. Bastiani, P. Canaran, J. Chan, W. J. Chen, P. Davis, J. Fernandes *et al.*, "Wormbase 2007," *Nucleic acids research*, vol. 36, no. suppl 1, pp. D612–D617, 2008.

[52] P. Gleeson, V. Steuber, and R. A. Silver, "neuroconstruct: A tool for modeling networks of neurons in 3d space," *Neuron*, vol. 54, no. 2, pp. 219 – 235, 2007. [Online]. Available: http://www.sciencedirect.com/science/article/pii/S0896627307002486

[53] "CElegansNeuroML," https://github.com/openworm/CElegansNeuroML, 2012–2016.

[54] C. Fang-Yen, C. V. Gabel, A. D. Samuel, C. I. Bargmann, and L. Avery, "Laser microsurgery in caenorhabditis elegans," *Methods in cell biology*, vol. 107, p. 177, 2012.

[55] P. B. Allen, A. E. Sgro, D. L. Chao, B. E. Doepker, J. S. Edgar, K. Shen, and D. T. Chiu, "Single-synapse ablation and long-term imaging in live c. elegans," *Journal of neuroscience methods*, vol. 173, no. 1, pp. 20–26, 2008.

[56] M. Peliti, J. S. Chuang, and S. Shaham, "Directional locomotion of c. elegans in the absence of external stimuli," *PLoS One*, vol. 8, no. 11, p. e78535, 2013.

[57] "Plus500," http://www.plus500.com/, 2014–2016.

[58] J. C. Way and M. Chalfie, "The mec-3 gene of caenorhabditis elegans requires its own product for maintained expression and is expressed in three neuronal cell types." *Genes & development*, vol. 3, no. 12a, pp. 1823–1833, 1989.

[59] E. L. Ardiel and C. H. Rankin, "Cross-referencing online activity with the connectome to identify a neglected but well-connected neuron," *Current Biology*, vol. 25, no. 10, pp. R405 – R406, 2015. [Online]. Available: http://www.sciencedirect.com/science/article/pii/S0960982215003966

[60] W. Li, Z. Feng, P. W. Sternberg, and X. S. Xu, "A c. elegans stretch receptor neuron revealed by a mechanosensitive trp channel homologue," *Nature*, vol. 440, no. 7084, pp. 684–687, 2006.

[61] E. R. Kandel, J. H. Schwartz, T. M. Jessell, S. A. Siegelbaum, and A. Hudspeth, *Principles of neural science*. McGraw-hill New York, 2000, vol. 4.

[62] D. Purves, G. J. Augustine, D. Fitzpatrick, L. Katz, A.-S. LaMantia, J. McNamara, and S. Williams, "Neuroscience," *Sunderland, Massachusetts, USA*, 2001.

[63] G. A. Carpenter and S. Grossberg, "A massively parallel architecture for a self-organizing neural pattern recognition machine," *Computer vision, graphics, and image processing*, vol. 37, no. 1, pp. 54–115, 1987.

[64] Z. Li, Y. Li, Y. Yi, W. Huang, S. Yang, W. Niu, L. Zhang, Z. Xu, A. Qu, Z. Wu *et al.*, "Dissecting a central flip-flop circuit that integrates contradictory sensory cues in c. elegans feeding regulation," *Nature communications*, vol. 3, p. 776, 2012.

[65] T. Kimoto, K. Asakawa, M. Yoda, and M. Takeoka, "Stock market prediction system with modular neural networks," in *Neural Networks, 1990., 1990 IJCNN International Joint Conference on.* IEEE, 1990, pp. 1–6.